Declassified by authority of NASA
Classification Change Notices No. 113
Dated ** 6/28/67

DECLASSIFIED
CONFIDENTIAL

NATIONAL AERONAUTICS AND SPACE ADMINISTRATION

TECHNICAL MEMORANDUM X-381

EXPERIMENTAL BEHAVIOR OF COMBUSTION PRODUCTS OF HEF-2 AND AIR DURING EXPANSION IN EXHAUST NOZZLES*

By J. R. Branstetter, W. B. Kaufman, and A. L. Smith

F-796

CR-1

SUMMARY

The performance of a boric-oxide-laden stream during expansion through exhaust nozzles of two sizes was investigated. HEF-2 (largely propylpentaborane) was burned in an 8-inch-diameter combustor coupled to a convergent-divergent nozzle. The larger nozzle (a simple converging type) was connected to the 28-inch-diameter afterburner of a simulated turbojet engine. JP-4 fuel was burned in the primary combustor and HEF-2 in the afterburner. The tests were conducted at a nozzle-inlet pressure of 2.5 to 3 atmospheres over a range of equivalence ratios from 0.3 to 1.0.

The results of both investigations were similar to those reported earlier for pentaborane fuel in the same small-scale apparatus, even though the combustion products were appreciably different. Trace amounts of condensed boric oxide vapor observed to occur near the nozzle throat in the pentaborane tests did not occur in either of the present tests. No effect of combustor or nozzle size on the performance was observed. Experimental results agreed with ideal performance in the region where B_2O_3 is entirely liquid (i.e., below 3200° R). The same agreement was obtained at temperatures above 3500° R where the oxide was in the all-vapor phase. In the two-phase region (3200° to 3500° R) the experimental data departed rapidly from the ideal frozen-expansion model as well as from the ideal equilibrium-expansion model when these models assume B_2O_3 as the major boron combustion product. In fact, the experimental data at the combustor exit indicated that vaporization was complete at a temperature of about 3500° R, whereas ideal performance predicted that temperatures in excess of 3800° R were needed for complete vaporization. This results in a fuel consumption 11 to 20 percent greater than predicted by the ideal frozen- and equilibrium-expansion models, respectively. However, when the vaporized combustion product was assumed to be metaboric acid rather than B_2O_3, the ideal values for a frozen-expansion process agreed very well with the experimental values.

*Title, Unclassified.

INTRODUCTION

Boron-containing fuels by virtue of their favorable chemical energy are capable of extending the range of jet-propelled aircraft (ref. 1). These fuels introduce some unique problems, one of which is the behavior of the boron products of combustion during expansion in the exhaust nozzle. Relatively minor variations in the thermodynamic and kinetic properties of the boron products of combustion greatly affect analytic results of thrust and fuel consumption. Unfortunately, the actual composition, thermodynamic properties, and kinetics of boron-oxygen-hydrogen systems are not completely nor accurately known. For this reason the NASA undertook an experimental investigation to determine the behavior of pentaborane-air combustion products during expansion in a convergent-divergent nozzle (ref. 2). The performance was compared with ideal performance, which assumed that the only boron combustion component present in significant quantity at the temperatures considered was boric oxide (B_2O_3).

A review of the results of that investigation will pinpoint most of the problems to be dealt with in this report:

(1) Within the combustor, boric oxide vapor required about 400° F supercooling before any condensed phase was observed.

(2) In the nozzle, the vapor did not condense to anywhere near the extent predicted for a phase equilibrium-expansion process.

(3) For all practical purposes, the liquid boric oxide particles remain in thermal and velocity equilibrium with the rest of the combustion products during expansion through the nozzle.

(4) The experimentally obtained specific fuel consumption agreed with ideal performance at combustion temperatures (below 3300° R) for which the boric oxide was essentially in an all-liquid state and at combustion temperatures (above 3600° R) for which the boric oxide was considered completely vaporized.

(5) The loss in nozzle performance due to oxide films adhering to the nozzle surfaces was negligible for nozzle wall temperatures above 800° F.

The inability of the boric oxide to condense in the combustor and in the nozzle (items (1) and (2)) affected performance greatly. For example, at a combustor temperature of 3600° R, specific fuel consumption

DECLASSIFIED

E-796

CR-1 back

was 20 percent greater than predicted for ideal equilibrium combustion and expansion of boric oxide products.

In order to determine whether the observations noted for pentaborane could be generalized upon, two additional investigations were undertaken, one in the small-scale pentaborane apparatus of reference 2 and the other in a full-scale engine apparatus. Because it was available in large quantity, HEF-2 containing over 65 percent monopropylpentaborane was selected for both tests. HEF-2 yields exhaust products appreciably different from those of pentaborane, in that considerably less B_2O_3 is formed per pound of fuel burned and, in addition, CO_2 is present. In the full-scale application, still different exhaust products were generated by burning HEF-2 downstream of a turbojet primary combustor fueled with hydrocarbon fuel. This large configuration also provided increased residence time for the boric oxide (thereby providing a nearer approach to equilibrium behavior) and reduced boundary-layer effects in the exhaust nozzle. In both investigations the fuel-air mixtures were burned to near completion to assure proper analysis of results. The tests were conducted at combustor pressure of $2\frac{1}{2}$ to 3 atmospheres and encompassed equivalence ratios of 0.3 to 1.0.

Recent "best value" thermodynamic data suggest that the combustion mechanism of boron fuels favors the formation of metaboric acid in the vapor phase rather than boric oxide; this could explain the discrepancy observed in the transition region in the pentaborane performance investigation. A theoretical model employing this suggested mechanism is compared with the experimental data obtained herein.

The present report employs the computational methods of reference 2 to determine the thrust and fuel consumption and to separate performance losses due to combustion inefficiency from performance losses due to lack of phase equilibrium.

APPARATUS AND EXPERIMENTAL PROCEDURE

Small-Scale Installation

General assembly. - A diagram of the experimental equipment is shown in figure 1. Combustion air was passed through a single can-type jet-engine combustor used as a preheater. The preheater was used to warm the apparatus and was never operated concurrently with HEF-2 flow. An insulated duct downstream of the preheater contained baffles that

evened the velocity profile and produced small-scale turbulence at the entry to the HEF injector. The combustion products discharged through the exhaust nozzle into a thrust barrel supported by flexible straps fastened to the top of the exhaust plenum. The exhaust gases were cooled and discharged into an exhaust duct maintained at about 0.25-atmosphere pressure. Except for the addition of a flexible seal between the exhaust nozzle and the thrust barrel, the apparatus was the same as described in reference 2.

Combustor and nozzle. - The combustor and the nozzle were fabricated separately and welded to a common flange that was bolted to the exit plenum (fig. 2). The combustor was $8\frac{3}{8}$ inches in diameter and 36 inches long. Cooling air was metered and fed into an annular passage surrounding the combustor by four ducts spaced 90° apart. The nozzle (fig. 2) was machined from a billet of mild steel, and its internal surfaces were nickel-plated to avoid corrosion. The nozzle was cooled by operating it as a heat sink; this cooling principle was satisfactory only because the tests were of short duration.

Warmup fuel (propylene oxide or JP-4) was injected from simple orifices immediately upstream of the HEF-2 injectors for high-temperature calibration and during warmup.

HEF-2 injector. - The fuel injector was designed to obtain strong and uniform mixing of the HEF-air mixture before combustion, on the premise that this is a prerequisite for high combustion efficiencies and uniform temperatures. Details of the injector are shown in figure 3. Atomizing air at near sonic velocity atomized the fuel to a fine mist, which was directed downstream at a 40° angle to the combustor axis. The combustion air was accelerated by blocking off about 88 percent of the duct area with plates inserted between the spray bars (fig. 4). The fuel injector was water-cooled so that HEF-2 flow could be initiated while the preheater was operating.

Fuel system. - The fuel systems and the method for supplying air for atomization of the fuel are shown in figure 5. The test-fuel system was flushed with dry JP-4 fuel immediately after each HEF-2 test.

Fuels. - Properties of the HEF-2, along with properties of pentaborane, are listed in table I. (The batch of HEF-2 used in the 8-in. combustor was manufactured at a much earlier date than that used in the afterburner. There is no correlation of composition and heat of combustion for these two fuels.) Propylene oxide and JP-4 fuel (warmup fuels) were used interchangeably for calibrating the apparatus and for warmup prior to the HEF-2 tests.

E-796

E-796

Instrumentation. - The combustion air, atomizing air, and cooling air were metered by sharp-edged orifices conforming to ASME standards. HEF-2 flow rates were sensed by two rotating-vane flowmeters, each of which was connected to a separate continuous recorder.

Barrel thrust was measured by a strain gage connected to a continuous recorder. A camera recorded at 5-second intervals the manometer-board readings, which consisted of orifice differential pressures, static pressures (stations shown in fig. 2), combustor-inlet total pressure, and exhaust-plenum pressure.

Thermocouple data from the air orifices, fuel meters, combustor inlet (station 2), combustor and nozzle walls (fig. 2), and cooling-air discharge were recorded every 6 seconds on self-balancing potentiometers. At the lower equivalence ratios investigated, radial-temperature profiles of the combustion products were obtained by means of a traversing thermocouple connected to a fast-response, self-balancing recording potentiometer. The thermocouple was mounted 8 inches upstream of the nozzle entry. A calibrated sonic-flow aspirating-type thermocouple (ref. 3) was used for the calibration tests and was replaced with an exposed-bead thermocouple for the HEF-2 tests.

Samples of the HEF-2 combustion products were obtained with a liquid-nitrogen-cooled probe immersed in the stream. Solids were trapped on glass-wool gauze, and the filtered gases flowed into an evacuated bottle. Operation of the apparatus was controlled by a remotely operated valve.

Procedure. - The procedures for calibrating the test apparatus and for conducting the HEF-2 tests are taken from reference 2. Each test was conducted in the following manner: The HEF-2 flowmeters and the thrust-barrel strain gage were calibrated. After combustion airflow was established, warmup fuel was introduced at the preheater and through the warmup-fuel orifices immediately upstream of the HEF-2 injector. Complete sets of data were taken at various fuel-air ratios that yielded combustor-outlet temperatures ranging from 600° to 2500° F. The data obtained in this manner were used to calibrate the apparatus. During the calibration all instruments were checked for proper functioning and the apparatus was tested for leaks. Next, the apparatus was cooled and the sonic-flow aspirating thermocouple was replaced with the open-bead thermocouple.

The combustor was preheated before injection of the test fuel. As soon as the HEF-2 flow was established, the warmup fuel was shut off. Air- and fuel-flow rates were quickly adjusted to predetermined values, and data were taken at these fixed flow rates for a period of at least 15 seconds. On most runs, the fuel-air ratio was then changed to a new

value, and the test was continued until the fuel was expended. In many cases, a combustion-product sample was obtained during the run. Sampling of the products, which required about 20 seconds, was begun shortly after the fuel-air ratio was set. (The samples were quantitatively analyzed for free hydrogen and free boron.)

After each test, the combustor, the nozzle, and the fuel injector were inspected and thoroughly cleaned. Measurements of the nozzle-throat diameter determined the amount of area change resulting from the large thermal stresses that occurred during the test.

Large-Scale Installation

General assembly. - The large-scale installation (fig. 6) consisted of a primary-combustor section of a turbojet engine, a mixing section, an afterburner, and a converging exhaust nozzle. Nonvitiated heated air was metered to the primary combustor where it was further heated with jet fuel to afterburner-inlet conditions. Either HEF-2 or JP-4 fuel could be burned in the afterburner. Ignition of the afterburner was by a "hot streak" initiated at the primary-burner outlet. The combustion products were cooled and scrubbed with water sprays. The gases were carried to the altitude exhaust system, while the scrubbing water and dissolved products were pumped to a settling basin.

Combustor and nozzle. - The afterburner was 10 feet long and had an inside diameter of 28 inches. The double-walled construction provided an annular passage for cooling air. No afterburner liner was needed.

The exhaust nozzle (figs. 7 and 8) was machined from mild-steel plates welded together. The inside surface was nickel-plated. Cooling air supplied to a manifold at the upstream end flowed through a 3/4-inch annular passage and was discharged in the plane of the nozzle exit.

Fuel injectors. - Fuel was injected at right angles to the airstream by the air-atomizing spray bars shown in figures 9 and 10. There were 12 ports per bar, six on each side, with 18 bars to a complete set. They were designed with these specific objectives in mind:

(1) To prevent HEF-2 from decomposing in the fuel tube. This requirement necessitated a considerable quantity of atomizing air as a coolant, particularly since the spray bars were located downstream of the flameholder.

(2) To prevent clogging of injection ports due to impingement of droplets on the inside edge of the air hole. Had the ports been two concentric holes, expansion of the outer tube relative to the inner tube

would have resulted in eccentricity in the alinement of the holes and impingement of the fuel jets. Therefore, a short tube extending through the atomizing-air hole was welded to the fuel-supply tube at each fuel port. The tubes and air holes were constructed eccentric to each other so that the expected expansion would bring them concentric.

(3) To obtain a well-atomized fuel spray. To preclude impingement of fuel on combustor walls and adjacent injectors and to vaporize the fuel as quickly as possible, near sonic velocity of the atomizing air at each injection port was desired.

(4) To obtain high combustion efficiency. Six pairs of injection ports per bar, 216 total points of injection, were felt to be the maximum number practical. Also, to achieve good combustion efficiency, a multigutter flameholder was selected. Location of the fuel-spray bars upstream of the flameholder then was impossible, since decomposed fuel and combustion products would accumulate on flameholder parts. The injection ports were therefore located downstream of but close enough to the gutter edges of the flameholder to spray fuel into the turbulent wakes of the gutters but far enough away to prevent recirculation of decomposed fuel and boric oxide into the gutters.

(5) To provide a flat temperature distribution across the combustor. The fuel ports were sized to give a constant fuel-air ratio across the plane of the injectors.

Fuel-manifold pressure at maximum flow rate of 1.25 pounds per second was about 50 pounds per square inch gage. Atomizing-air flow averaged about 1.5 pounds per second at a manifold pressure of 80 pounds per square inch gage. JP-4 fuel was also burned from these injectors during warmup and calibration.

Flameholder. - The downstream edges of the circular V-gutters were in the same plane (figs. 9 and 10). The hollow tubes between gutters and the center cone were simple modifications to the original flameholder to provide increased blockage. Equally distributed blockage of the combustor cross-sectional area would have brought the outer gutter too close to the combustor wall. Short radial V-gutters were included between the second and third gutters and extended beyond the outer gutter to make up some of this blockage. The total blockage amounted to 77 percent of the combustor cross-sectional area.

Fuel system. - The fuel system was essentially the same as that described earlier for the small-scale apparatus, with one exception. The JP-4 fuel line to the afterburner was teed to the HEF-2 line where it entered the afterburner fuel manifold. Hence, afterburner warmup was obtained by injection of JP-4 fuel through the HEF-2 injectors.

Instrumentation. - Combustion-air flow was measured by a calibrated Venturi; atomizing-air, afterburner cooling-air, and nozzle cooling-air flows were measured with sharp-edged orifices. Fuel-flow rates were measured by rotating-vane flowmeters. Temperatures were taken at the fuel and air measuring stations and at the afterburner-inlet station. Total and static pressures were taken at the afterburner inlet; total pressures were also taken through a water-cooled rake at the nozzle inlet.

The exhaust-nozzle instrumentation consisted of 48 Chromel-Alumel skin thermocouples, 48 static-pressure taps, four lip static-pressure taps, and eight thermocouples at the cooling-air inlet and outlet. The skin thermocouples were divided evenly between two rows spiraling axially through the nozzle 180° apart. The axial locations of the thermocouples are indicated in figure 7. The static-pressure taps were located in two rows displaced 90° from the thermocouples but at the same axial stations.

All pressures, temperatures, and fuel flows were recorded on an automatic digital data-reduction system.

Procedure. - The large-scale test runs were conducted as follows: The proper airflows were established to the primary combustor, afterburner cooling shell, and exhaust-nozzle cooling shell. When an inlet air temperature of 1060° R was reached, the primary combustor was ignited. JP-4 fuel flow was increased until the primary-burner outlet temperature was 2000° R. This temperature was held constant for the remainder of the test. Check-point data on primary-burner performance were recorded at this point. Atomizing-air flow to the afterburner fuel injectors was set, and JP-4 fuel was introduced and ignited by the hot streak. The exhaust back pressure was reduced to about 1/2 atmosphere. Afterburner fuel flow was increased to a predetermined fuel flowmeter setting to give 2660° R. Airflow was adjusted until the afterburner-inlet static pressure was 5000 pounds per square foot. Check-point data on afterburner JP fuel performance were then recorded. The HEF-2 tank was pressurized; and, as HEF-2 was throttled into the afterburner fuel manifold, JP-4 was throttled out. Nozzle-inlet temperatures were stabilized at desired levels between 2700° and 3900° R by adjusting HEF-2 flow to predetermined flowmeter settings. A constant afterburner static pressure of about 5000 pounds per square foot was maintained. A continuous purge of all pressure taps was interrupted only during the 30 seconds required to record the pressures.

DECLASSIFIED
CONFIDENTIAL

ANALYTIC PROCEDURE

Calculations

The principal quantities calculated from the data were thrust at the nozzle throat F_8, thrust at the nozzle exit F_{15} in the case of the small-scale nozzle, and combustion efficiency η_c. (See appendix A for a listing of symbols.) A detailed description of the computation method is given in reference 2. Combustion-efficiency computations are naturally quite sensitive to the composition and enthalpy content of the exhaust products. The analytic procedure assumes that the boron is in the form of B_2O_3 and that it does not dissociate. The other products are assumed to be at composition equilibrium at the combustor exit but at a frozen state in the nozzle.

The total temperature at the nozzle throat T_8, herein called the experimental temperature, is computed from the continuity equation for measured values of pressure and weight flow:

$$T_4 = T_8 = \frac{(P_4)^2}{R_8}\left(\frac{A_N C_d C_k}{w_t}\right)_8^2\left[\frac{\gamma g}{\left(\frac{\gamma+1}{2}\right)^{\frac{\gamma+1}{\gamma-1}}}\right]_8 \tag{1}$$

The nominal area A_N requires correction factors that account for boundary-layer film and nozzle-wall curvature C_d and thermal expansion of the wall C_k. For each nozzle, the coefficient C_d was computed by means of reference 4 and is presented in figure 11; C_k for the converging nozzle was determined from nozzle wall temperatures and ASME nozzle standards; C_k for the converging-diverging nozzle was computed from the measured pressures, temperatures, and flow when burning warmup fuel (see fig. 12).

The properties R and γ change with the amount of liquid and vapor present in the mixture as well as with the equivalence ratio:

$$R = R_g \frac{w_g}{w_t} = R_g\left(1 - \frac{w_l}{w_t}\right) \tag{2}$$

and

$$\gamma = \frac{\Sigma n C_p}{\Sigma n C_p - 1.987\ \Sigma n_g} \tag{3}$$

where the sum is taken over components of the mixture. Equations (2) and (3) are developed basically in the same manner as given in reference 5. The quantities involved are evaluated at the static temperature of the throat:

$$t_8 = \left(\frac{2T}{\gamma + 1}\right)_8 \tag{4}$$

The combustion efficiency is defined as the enthalpy rise across the combustor divided by the heat of combustion:

$$\eta_c = \frac{H_8 + \left(h_v \frac{w_v}{w_a}\right)_8 + \frac{q}{w_a} - H_3}{\Sigma h_c f} \tag{5}$$

The equation assumes that the entire combustion process occurs downstream of station 3. The basis is 1 pound of air. The term q accounts for the heat transferred to the coolant between stations 3 and 8, H_3 is the enthalpy of all the incoming air and fuel, and H_8 is the enthalpy of the products exclusive of the latent heat of vaporization of the boric oxide.

Equations (1) to (5) permit the evaluation of T_8 and η_c when the fraction of boric oxide in the vapor state is known. Conversely, equation (5) can be used to determine the ratio of liquid to vapor oxide if η_c is known.

The experimentally determined stream thrust at the nozzle throat (sum of a pressure term and a momentum term) is

$$F_8 = F_{8,id} C_M = P_4 (A_N C_M C_k)_8 \left[\frac{\gamma}{2^{\gamma-1}(\gamma + 1)^{\frac{1}{1-\gamma}}}\right]_8 \tag{6}$$

For each nozzle, the coefficient C_M, which includes the effects of nonuniform flow in the mainstream and the boundary layer, is computed by means of reference 4 and is presented in figure 11. In the case of the convergent-divergent nozzle, the experimentally obtained stream thrust at the nozzle exit is

$$F_{15} = F_8 + (\Sigma pA)_D - \Delta F_{id} C_{fr} \tag{7}$$

where the axial force on the divergent surface of the nozzle ΣpA is obtained from static-pressure measurements along the nozzle surface,

and ΔF_{id} is the ideal one-dimensional stream-thrust increase between the throat and the exit. The ratio of the thrust increase to the ideal thrust

$$\frac{\Delta F_{id}}{F_{8,id}} = \frac{\Delta F_{id}}{F_8/C_M} \tag{8}$$

and is plotted in figure 13.

The friction coefficient C_{fr} is shown in figure 11. The performance of the nozzle divergence (omitting friction terms) is defined as

$$\eta_w = \left(\frac{\Sigma pA}{\Delta F_{id}}\right)_D 100 \tag{9}$$

and is presented on figure 14 for warmup-fuel products of combustion.

For each nozzle, an alternative means of measuring the thrust was employed. For the convergent-divergent nozzle, the exit thrust as determined by the thrust barrel $F_{15,bb}$ is the sum of the strain-gage force and a smaller force stemming from the axial body forces acting on the outer surface of the thrust barrel. (The subscript bb will be used throughout the report to differentiate between the two methods of evaluating the nozzle-exit stream thrust.) For the convergent nozzle, the alternative method of thrust measurement was to employ a momentum envelope within the exhaust nozzle. The exit thrust here is

$$F_{8,en} = \frac{F_4 - (\Sigma pA)_C}{1 + C_{fr}} \tag{10}$$

where C_{fr} for the convergent nozzle was taken to be 0.003.

Performance Analysis

The method of analysis of the data obtained with each apparatus closely parallels the analysis method employed for the pentaborane data (ref. 2). The combustion efficiency is obtained from the experimental temperature (eq. (1)). The method is as follows.

If equation (5) and all other equations containing terms affected by the composition of the combustion products are to be solved, the ratio of vaporized to total boric oxide must be known. Actually, two methods are available for determining the amount of vaporized boric oxide. In the conventional method, the amount of oxide vapor is defined

by the ideal equilibrium vapor-pressure data. Because this method makes the oxide phase and the combustion efficiency dependent on the vapor-pressure data (ref. 2), an indirect method of making the determination was used. The boric oxide was assumed to be all in the liquid phase at the lowest equivalence ratios tested and all in the vapor phase at the highest equivalence ratios tested. These assumptions permitted a direct solution of all the equations. The computed combustion efficiencies of the fuel at both the lowest and highest equivalence ratios tested were found to be a constant value. This value of combustion efficiency was therefore assumed to exist at intermediate values of equivalence ratio where the boric oxide was in a mixed phase at the nozzle throat. With the combustion efficiency specified, the amount of oxide in each phase could be computed by a trial-and-error solution of equations (1) to (5).

Thrust equations (6), (7), and (10) assume that the oxide film on the nozzle surfaces is smooth and of negligible thickness so that the area of the throat and the value of C_{fr} are unaffected. Thrust values obtained from the thrust barrel are applicable for even the thickest films. Therefore, a comparison of F_{15} (values from eq. (7)) and $F_{15,bb}$ provides means of measuring the effect of the films on thrust. Also, the two methods provide a check on the accuracy of the convergent-divergent nozzle data as a whole. As noted in appendix B, the $F_{15,bb}$ data were less precise than the F_{15} data; consequently, the F_{15} values are of the greater accuracy when oxide films are not an influencing factor.

In order to clarify the comparison between experimental data and the theoretical (ideal) data, the experimental data were reduced to a base of unit airflow, zero heat loss through the burner wall, and a constant inlet air temperature. The theoretical data were corrected for three-dimensional flow in the nozzle but omitted any correction for friction. The methods used are as follows:

(1) Ideal performance, based on unit airflow, is

$$S_{a,id} = \frac{F_{8,id}}{w_a} = \frac{[pA(1+\gamma)]_{8,id}}{w_a} = (1+f)\left[\sqrt{\frac{Rt}{\gamma g}}\,(\gamma+1)^2\right]_8 \qquad (11)$$

and

$$\left(\frac{F_{15}}{w_a}\right)_{id} = S_{a,id}\left[1 + \frac{\eta_w}{100}\left(\frac{\Delta F}{F_8}\right)_{id}\right] \qquad (12)$$

A value of 76 (fig. 14) was used for η_w. The ideal impulse data were computed for an inlet air temperature of 360° R for the convergent-divergent nozzle and 844° R for the convergent nozzle.

DECLASSIFIED

(2) The experimentally obtained data reduced to a unit airflow base are

$$S_a = \frac{F_8}{w_a}$$

$$\frac{F_{15}}{w_a} = \frac{F_8 + (\Sigma pA)_D - \Delta F_{id} C_{fr}}{w_a} \tag{13}$$

(3) The experimentally obtained data were corrected to the inlet air temperature of 360° R (or 844° R) as follows:

$$\varphi_{corr} = \varphi - \left[\frac{T_{3,corr} - 360 \text{ (or } 844)}{f_{\varphi=1} h_c}\right] c_{p,3} \tag{14}$$

where

$$T_{3,corr} = T_3 - \frac{q}{w_a c_{p,3}}$$

This method is analogous to the method of reference 2, wherein the correction was applied to the thrusts and temperatures rather than φ.

RESULTS AND DISCUSSION

It should be emphasized that the techniques used to obtain the experimental results were selected because of their relative insensitiveness to the choice of thermodynamic values used in the data-reduction process. In contrast, relatively minor variations in the thermodynamic and kinetic data for the combustion product can have a pronounced effect on ideal analyses and hence on the values of combustion efficiency obtained. Likewise, any other interpretation of the experimental data that uses an ideal performance yardstick is suspect. The same thermodynamic data (refs. 6 and 7) utilized in reference 2 to compute the experimental and ideal performance were used in this report.

Values for the thermodynamic properties of boron compounds at elevated temperatures have undergone continuous revision during the course of this study; however, it is only fitting and proper that the experimental results obtained in the manner outlined previously be compared with the ideal results obtained by means of the most recent "best value" data. One such comparison is given in the section "Most Recent

Thermodynamic Data." Since even these recent data are subject to change, recomputation of all the results on the basis of these best-value data was not undertaken.

Test data for the small-scale engine are presented in tables II to IV; test data for the large-scale engine are presented in tables V and VI. At the lower temperatures encountered in these tests, the combustion products contained liquid boric oxide particles. Since the products are not completely gaseous, the use of perfect-gas, one-dimensional-flow equations to obtain the performance parameters may be questionable. Therefore, before the performance parameters are discussed, results that justify this method of analysis will be presented.

The combustion products from hydrocarbon fuel are "clean"; that is, they are completely gaseous. A comparison of the thrust F_8 obtained from equation (6) using one-dimensional isentropic expansion at constant γ with the "actual" thrust $F_{8,en}$ obtained from a summation of the measured pressures within the nozzle is shown on figure 15. The ideal thrust for the clean products of JP-4 is within 0.4 percent of the "actual" thrust. This shows that the terms that can enter into equation (6) are applied correctly for hydrocarbon combustion products.

That equation (6) is just as valid for boron-fuel combustion products is also illustrated in figure 15. The same good agreement between F_8 and $F_{8,en}$ was obtained for the mixture of HEF-2 and JP-4, even though the combustion products were not clean.

From the preceding discussion it is apparent that a modified one-dimensional isentropic analysis is justified for the nozzle as a whole. It is evident in figures 16 to 18 that the change of pressure with area at each station in the nozzle is the same for boron combustion products as for hydrocarbon products. This result shows that these products at all stations in the nozzle behave as a perfect gas expanding in a frozen state. Therefore, both in the overall expansion and in the incremental expansion, the data exhibit a frozen-expansion type of behavior; that is, (1) at temperatures where the boric oxide is all-liquid, this liquid remains fixed in quantity and is at temperature and velocity equilibrium with the gaseous products; and (2) at temperatures where the boric oxide is appreciably or totally vaporized, there is no change in phase or composition within the nozzle.

These results are identical with those for pentaborane (ref. 2), with one exception: Trace amounts of condensation were observed near the nozzle throat with pentaborane at several of the fuel-air ratios investigated. This was evidenced by an abrupt shift in pressure ratio in the region of condensation. In the present investigation no such deviation was observed. The absence of condensation could be attributed to the lower concentration of oxide present.

E-796

DECLASSIFIED

The use of equation (1) to obtain the temperature of the product is justified on the grounds that it was developed from the same basic assumptions of thermodynamic state and process as was equation (6). However, an error in the experimental temperature can be introduced by improper selection of R_8 and γ_8. The largest error would be expected if the boron product were assigned to the wrong phase. Using the 3500° R temperature level of the afterburner as an example, the all-liquid boric oxide state yields a 30° R higher temperature than does the all-vapor state. On the other hand, if the combustion products at the higher temperatures (all vapor) had been assumed to be those of the most recent best-value thermodynamic data, the resulting experimental combustion temperature would deviate only a few degrees from the experimental temperature obtained for boric oxide vapor.

E-796

These investigations were concerned primarily with the behavior of the oxide-laden gases in exhaust nozzles; consequently, little was done with the combustors other than to provide a reasonably flat exit-temperature distribution and a combustion efficiency near 100 percent.

Typical exit-temperature profiles are plotted in figure 19. While neither profile was as flat as desired, the 300° to 400° spread was not considered serious. The decrease in temperature toward the center of the afterburner was probably due to plugging of the inner two or three fuel ports on most of the spray bars with thermally decomposed HEF-2.

Combustion Efficiency

The combustion efficiencies for the 28-inch-diameter afterburner are shown in figure 20. Two efficiencies were calculated for each data point; one assuming an all-liquid boric oxide and the other assuming an all-vapor boric oxide. The combustion efficiency at low equivalence ratios, where the oxide was in the all-liquid state, and at high equivalence ratios, where the oxide was all vaporized, was 100 percent. These data and the 8-inch-diameter combustor data are summarized as follows:

Fuel	Combustion efficiency, η_c, %	
	All-liquid	All-vapor
HEF-2 (8-in.-diam. combustor)	97	97
HEF-2 + JP-4 (28-in.-diam. afterburner)	100	100
Pentaborane (ref. 2)	100	100

Introduction of current best values for the thermodynamic properties of the boron product would yield slightly higher combustion-efficiency values in the all-vapor column (see later discussion).

There is no reason to suspect a variation from the above-tabulated end values in the indeterminate two-phase region. This reasoning is substantiated by heat-balance data of reference 8 and by results of exhaust-gas sampling in the 8-inch combustor. In this two-phase region it is a simple operation to determine what fraction of the B_2O_3 must be in the condensed state to yield the combustion efficiency obtained at the end states. The fractions of boric oxide condensed, calculated in this manner, are presented in the tables and at the top of figures 21 to 25.

A decrease in combustion efficiency at the highest equivalence ratio tested can be observed from figure 20 for the mixture of HEF-2 and JP-4. At equivalence ratios near unity, combustion efficiency fell to 84 percent for HEF-2 alone (table IV). Similar results were observed in reference 8. These observations are attributed (ref. 2) to insufficient mixing of the fuel and air prior to combustion. Reference 2 showed that, when the mixing intensity was increased, the point at which efficiency began to drop off shifted to a higher equivalence ratio.

Combustor-Exit Temperatures

The ideal and experimental combustor-outlet temperatures are plotted in figures 21 and 22. For the combustion of HEF-2, figure 21 shows that, below an equivalence ratio of 0.506, the experimental data follow the ideal curve for all-liquid boric oxide but lie about 3 percent below it. A similar departure can be observed in the all-vapor region above an equivalence ratio of 0.715. The 3-percent deviation is probably a reflection of the combustion efficiency (97 percent for the 8-in.-combustor tests).

The experimental temperature (fig. 21) at which small amounts of vapor are observed agrees, within the 3-percent deviation, with the ideal temperature of 3200° R. As the equivalence ratio is increased from this point, a discrepancy arises and becomes a maximum at an equivalence ratio of 0.715, where the experimental data indicate that vaporization is complete, whereas theoretically only 60 percent of the oxide should be vaporized. The experimental temperature for complete vaporization (3550° R) was about 400° below that theoretically predicted (3940° R).

Similar conclusions can be drawn from the afterburner data presented in figure 22. In this case the oxide concentration at a given

temperature was lower than in the case just discussed, since JP-4 fuel was burned in the primary combustor at the same time that HEF-2 was being burned in the afterburner. For this reason the discrepancy between ideal and experimental curves in the two-phase region is not as great as for HEF-2 alone. The results obtained from figures 21 and 22 compare favorably with the pentaborane results of reference 2 in that the ideal data show that only about half the boric oxide is vaporized at the equivalence ratio where the experimental data show complete vaporization.

E-796

Air Specific Impulse

Air specific impulse for the 8-inch- and the 28-inch-diameter engines is plotted in figures 23 and 24, respectively. Four ideal models are included. Both the equilibrium- and frozen-expansion models assume that phase equilibrium exists at the nozzle inlet. A comparison of the impulse data and combustor-exit temperature data for each engine indicates that the actual products are characterized by a frozen-expansion process. This is the same result that was arrived at on the basis of the pressure-ratio data (figs. 17 and 18). In the two-phase region, the departure of the ideal-frozen curve from the ideal-equilibrium curve increases with Mach number, as illustrated by comparing figures 23 ($M = 1$) and 25 ($M > 1$). Since the actual products are observed to continue expanding in a frozen manner in the divergent section of the small nozzle, the departure of the experimental data from the ideal equilibrium expansion data becomes very sizable at the nozzle exit. For example, at an air specific stream thrust of 166 seconds, the actual fuel consumption is over 20 percent greater than the ideal-equilibrium value. Only a small fraction of this is traced to combustion inefficiency. The remainder is divided between the performance defect observed in the combustor (fig. 22) and the inability of the vaporized boric oxide to condense in the nozzle.

CR-3

A comparison of experimental and ideal fuel consumption for several fuels based on the thrust level at the nozzle throat is shown in figure 26. The experimental data are corrected to 100-percent combustion efficiency, and the ideal performance data are for the frozen-expansion model. Below an air specific impulse of 140 seconds (low-temperature, all-liquid region), the deviation of experimental from ideal performance is within experimental error. As vaporization temperatures are reached, the deviation increases until, at air specific thrust levels of 152 seconds, 11 percent more fuel would be consumed by an engine such as a ramjet operating on HEF-2 than predicted by this theoretical model. About half as much deviation can be observed for a turbojet engine with afterburner, since only part of the enthalpy rise is contributed by the HEF-2-fueled afterburner.

Regardless of the theoretical considerations, the fact remains that, because of the nature of the combustion products of boron-containing fuels, thrust levels requiring combustion temperatures above 3200° R are realized only at considerable expense in fuel consumption. For instance, at an equivalence ratio of 0.525 (fig. 25), a 7-percent increase in stream thrust would require a 36-percent increase in fuel consumption. In other words, no additional thrust is derived from over half the fuel required to increase the combustor-outlet temperature from 3200° to 3550° R. Careful consideration should be given this observation in the application of boron-containing fuels to ramjets and afterburners that will operate in this temperature range.

Most Recent Thermodynamic Data

The thermodynamic data for the combustion products of boron-containing fuels, particularly the vapor pressure of the oxide, have undergone several changes in the past few years. The most consistent set for B_2O_3 products was used in the calculations herein. However, studies recently reported indicate the major product formed from B_2O_3 liquid at elevated temperatures in the presence of water vapor is metaboric acid (HBO_2) rather than boric oxide vapor (B_2O_3). Even in these "best value" data there is considerable latitude in choice of values. Ideal combustion temperatures were calculated for HBO_2 product based on a value of 132.5 kilocalories per mole for the formation of HBO_2 chosen from the lower limit given in reference 9. The results are plotted in figure 27 for comparison with ideal B_2O_3 data and the experimental data of figure 22. The small difference between the two all-vapor curves is due to the difference in the heat absorbed in vaporizing B_2O_3 compared with that absorbed in the formation of HBO_2. The all-liquid curves are identical, since liquid B_2O_3 precedes the formation of HBO_2.

An important result to be observed from this plot is the difference in the two phase-equilibrium curves for the ideal data. The displacement of these two curves is due to the difference in the vapor pressures, that of HBO_2 being the higher. The formation of HBO_2 begins at a temperature of about 2800° R, some 400° below that at which vaporization of B_2O_3 begins. The temperature for complete vaporization is very nearly the same for both products, about 3750° R. The experimental data are observed to lie much closer to the HBO_2 curve than to the B_2O_3 curve. In view of this result, the assumption that HBO_2 is the major combustion product above 2800° R appears to be a valid one.

E-796
CR-3 back

Oxide Films

The presence of boric oxide films on the nozzle surfaces presents two basic problems. Oxide films decrease nozzle throat area and hence yield inaccuracies in thrust and temperature data, F_8 and T_4, respectively. Surfaces roughened by the viscous oxide (6000 poises at 1000° F) incur frictional losses. This report utilizes the techniques successfully employed in reference 2 to ascertain the film thickness at the throat and the thrust loss attributed to surface roughness.

All convergent-divergent nozzle data were screened to ensure that the film thickness at the throat was negligible. This screening operation discarded some data points obtained at throat-wall temperatures below 1000° F, the danger-point temperature reported in reference 2. Several examples of thrust loss incurred by oxide films on the nozzle divergence are shown in figure 28. The loss is observed to increase during the first 20 seconds of testing as the film grows to equilibrium thickness. The highest frictional losses are associated with the lowest equivalence ratios. Difficulty was encountered in operating at nozzle-wall temperatures as high as those obtained in the pentaborane tests. However, the present data are in good agreement with the pentaborane tests, which showed thrust losses amounting to as much as 6 percent when the divergent wall temperatures were below 800° F.

In the large nozzle (afterburner tests), wall temperatures (table V) were always well above the danger point. As expected, there were no observable film effects on the data.

SUMMARY OF RESULTS

Investigation of the behavior of combustion products of HEF-2 and of HEF-2 and JP-4 expanding through a small-scale convergent-divergent exhaust nozzle and a full-scale convergent exhaust nozzle yielded the following results:

1. The behavior of the exhaust products in the subsonic and sonic flow regions appeared independent of nozzle size. The liquid particles remained in thermal and velocity equilibrium with the rest of the combustion products. Liquid boric oxide films had a negligible effect on performance for the wall temperatures encountered in this investigation.

2. Although the performance level varied with the fuel used, the thermodynamic and kinetic behavior of the combustion products appeared to be independent of the type of fuel (i.e., whether the fuel was HEF-2, mixture of HEF-2 and JP-4, or pentaborane of ref. 2).

3. Condensation of vaporized boron products did not occur within either nozzle.

4. The experimental results agreed with the ideal performance, within the 3-percent limit of combustion efficiency, in the region below 3200° R. Below 3200° R the boron constituent in the combustion gases is in the liquid phase.

5. The experimental results and ideal performance (based on an all-vapor product) also agreed in the region above 3500° R where the boron constituent was found to be in the all-vapor phase.

6. In the two-phase region (3200° to 3500° R), the experimental data showed a large departure from ideal values based on (1) an equilibrium state at the nozzle inlet and (2) boric oxide as the major combustion product. When the vapor was assumed to be metaboric acid, the ideal combustion temperatures showed good agreement with the experimental data.

7. Ideal performance predictions based on frozen expansion of boric oxide product (HEF-2) can be as much as 11 percent higher than can actually be attained by engines operating at nozzle-inlet temperatures above 3200° R.

8. Oxide films on the divergent surface of the small nozzle yielded thrust losses as great as 6 percent; losses of this order had been predicted (ref. 2) if wall temperatures dropped below 800° F.

Lewis Research Center
National Aeronautics and Space Administration
Cleveland, Ohio, May 13, 1960

DECLASSIFIED

E-796

APPENDIX A

SYMBOLS

A	area, sq in.
A_N	cross-sectional area of nozzle throat at 70° F
C_d	coefficient of discharge
C_{fr}	coefficient of friction
C_k	thermal expansion coefficient
C_M	momentum coefficient
C_p	molar specific heat at constant pressure, Btu/(lb-mole)(°R)
c_p	weight specific heat at constant pressure, Btu/(lb)(°R)
F	stream thrust, lb
ΔF	actual thrust change between nozzle throat and exit, lb; $\Delta F = F_{15} - F_8 = (\Sigma pA)_D$ - friction
ΔF_{id}	thrust change between nozzle throat and exit for one-dimensional isentropic flow of an ideal gas
f	fuel-air ratio
g	gravitational constant, 32.17 ft/sec^2
H	enthalpy per pound of air, Btu/lb
h_c	heat of combustion, Btu/lb
h_v	heat of vaporization of boric oxide, Btu/lb
M	Mach number
n	number of moles
P	total pressure, lb/sq in. abs
p	static pressure, lb/sq in. abs

ΣpA	axial pressure force on internal surface of nozzle obtained by graphical integration of wall static pressure against cross-sectional area, lb
q	heat rejected to coolant, Btu/sec
R	fluid constant, ft-lb/(lb mixture)(^{o}R)
S_a	air specific impulse, lb stream thrust/(lb air)(sec)
T	total temperature, ^{o}R
t	static temperature, ^{o}R
V	velocity, ft/sec
w	weight-flow rate, lb/sec
γ	ratio of specific heats
η_c	combustion efficiency
η_w	divergence efficiency for small-scale nozzle, $(\Sigma pA/\Delta F_{id})_D$ 100
φ	equivalence ratio

Subscripts:

a	air
bb	thrust barrel
C	convergence
corr	corrected
D	divergence
en	envelope
ex	experimental
f	fuel
g	gas
id	ideal

DECLASSIFIED

l	liquid
t	total
v	vapor

Numerical subscripts denote axial position (figs. 1, 2, and 6); specifically:

2	upstream of test-burner fuel injectors
3	downstream of fuel injectors and prior to any combustion
4	combustor exit
8	nozzle throat
15	nozzle exit

APPENDIX B

ACCURACY OF EXPERIMENTAL RESULTS

Small Scale

The method by which the small-scale apparatus was calibrated using warmup-fuel and air products of combustion is described in detail in reference 2.

The calibration data were used to determine the following:

(1) Expansion of the nozzle-throat area C_k

(2) Divergence efficiency of perfect gases in the nozzle divergence η_w

(3) Accuracy of T_8, η_c, F_8, F_{15}, and $F_{15,bb}$ for completely gaseous exhaust products

Because of the thrust-barrel alterations that reduced the heat flux in the nozzle block, the C_k values presented herein differ somewhat from those of reference 2.

Data accuracy statements (based on an overall analysis of all the data) of reference 2 are applicable to these data with two exceptions:

(1) The stream thrust values ($F_{15,bb}$) obtained with the thrust barrel, while still lacking the degree of accuracy (99 percent) cited for stream thrust F_8 and F_{15}, are considered to be in error by no more than 1.5 to 2 percent.

(2) Static-pressure measurements along the nozzle surfaces for HEF-2 products are subject to somewhat greater error than for pentaborane because of greater tendency for the holes to become fouled with oxides. In the convergent section, the error is less than 1 percent; in the aft portion of the divergent section, the error may be as great as 10 percent.

Emphasis must be placed on the fact that the combustion temperatures obtained from equations (1) and (4), as well as the combustion-efficiency data, are subject to error depending on the extent the thermodynamic data depart from the actual thermodynamics of the combustion products. Temperature errors arising from thermodynamic property variations are discussed in the RESULTS AND DISCUSSION section. The experimentally obtained thrust data are essentially independent of this type

of error. For example, a 5-percent change in the value of γ in equation (7) will change the stream thrust F_{15} by only 0.5 percent.

Large Scale

Airflow rates in the large-scale apparatus were measured within an error of 1 percent. Fuel-flow rates were measured within an estimated error of 0.5 percent. Combustor-exit total-pressure data and the nozzle static-pressure data contained errors in the order of 0.1 percent. In some cases, total-pressure readings were affected by oxide deposits. When this occurred, static-pressure data on the upstream portion of the nozzle were corrected to the total pressure at station 4 by applying a mean static- to total-pressure ratio obtained from ideal-gas, one-dimensional isentropic flow relations.

Accuracy of data for the large-scale apparatus was considered to be comparable to or better than the accuracy of the smaller apparatus. This is primarily attributed to more accurate determination of nozzle-throat area at operating temperature.

E-796

REFERENCES

1. Setze, Paul C., and Barnett, Henry C.: A Review of NACA Research Through 1957 on Boron Compounds as Fuels for Jet Aircraft. NASA MEMO 10-7-58E, 1958.

2. Branstetter, J. Robert, and Setze, Paul C.: Experimental Behavior of Pentaborane-Air Combustion Products During Expansion in a Convergent-Divergent Nozzle. NACA RM E57I20, 1958.

3. Glawe, George E., Simmons, Frederick S., and Stickney, Truman M.: Radiation and Recovery Corrections and Time Constants of Several Chromel-Alumel Thermocouple Probes in High-Temperature, High-Velocity Gas Streams. NACA TN 3766, 1956.

4. Streiff, M. L.: Exit-Nozzle Design. APL/JHU TG 154-13, ch. 13 of Ramjet Technology, Appl. Phys. Lab., The Johns Hopkins Univ., 1953. (Contract NOrd 7386 with Bur. Ord., Dept. Navy.)

5. Fivel, Herschel J., Tower, Leonard K., and Gibbs, James B.: Pentaborane Combustion Performance in 9.75-Inch-Diameter Ram-Jet Engine in Connected-Pipe Altitude Facility. NACA RM E54I16, 1957.

6. Setze, Paul C.: A Review of the Physical and Thermodynamic Properties of Boric Oxide. NACA RM E57B14, 1957.

7. Huff, Vearl N., Gordon, Sandford, and Morrell, Virginia E.: General Method and Thermodynamic Tables for Computation of Equilibrium Composition and Temperature of Chemical Reactions. NACA Rep. 1037, 1951. (Supersedes NACA TN's 2113 and 2161.)

8. Falk, F., Rice, J. L., and Sigillito, V.: Combustion Characterisitcs of Boron-Based High Energy Fuels. Prog. Rep. No. 3, Feb. 15 - May 15, 1959, TG-315-3, Appl. Phys. Lab., The Johns Hopkins Univ., July 28, 1959. (Contract NOrd 7386.)

9. White, D., Walsh, P. N., Mann, D. E., and Sommer, A.: Thermal Functions and Heats of Formation of Some of the Major Vapor Species in the Boron-Oxygen-Hydrogen System at Elevated Temperatures. Tech. Rep. No. 4, Res. Foundation, The Ohio State Univ., July 1959. (Contract NOnr-495(12).)

DECLASSIFIED

E-796
CR-4 back

TABLE I. - FUEL PROPERTIES

	8-Inch combustor	28-Inch afterburner
HEF-2		
Heat of combustion as obtained in a bomb calorimeter (H_2O vapor, B_2O_3 crystal), Btu/lb	23,350	24,500
Composition (data supplied by manufacturer), percent by weight:		
Monopropyl pentaborane	72	66.0
Dipropyl pentaborane	24	13.0
Pentaborane	3	0.6
Other	1	20.2
Elemental composition (used in computing performance), percent by weight:		
Boron	48.82	46.6
Carbon	36.86	39.8
Hydrogen	14.32	14.2
Stoichiometric fuel-air ratio	0.0726	0.0726
Pounds of boric oxide per pound of fuel	1.57	1.57
Specific gravity	0.73	0.73
Pentaborane (B_5H_9)		
Heat of combustion (H_2O vapor, B_2O_3 crystal), Btu/lb	29,100	------
Stoichiometric fuel-air ratio	0.0763	------
Pounds of boric oxide per pound of fuel	2.76	------

CONFIDENTIAL

TABLE II. - PRIMARY DATA FOR NOZZLE OF 8-INCH-DIAMETER COMBUSTOR

Run (a)	Equivalence ratio, ϕ	Fuel flow, w_f, lb/sec	Primary-air flow, w_a, lb/sec	Atomizing-air flow, lb/sec	Combustor-inlet total press., P_2, lb/sq in.	Combustor-inlet velocity, V_2, ft/sec	Primary-air temp., T_3, $^\circ R$	Fuel-injector press.-loss ratio, $\frac{P_2 - P_4}{P_2}$	Combustor-exit total press., P_4, lb/sq in.	Area of nozzle throat at 70° F, A_N, sq in.	Duration of data point, sec	Cooling-air flow, lb/sec	Heat rejected to coolant, q, Btu/sec (b)	Combustor wall temp., °F	Nozzle wall temperature, °F				Internal force exerted on divergence of nozzle, $\sum pA$, lb	Nozzle-exit stream thrust measured by thrust barrel, $F_{15,bb}$, lb
															Station					
															5	8	11	14		
[c]7	0.6280	0.210	4.37	0.23	48.4	59.0	642	0.060	44.50	12.30	40	4.80	203	1220	1450	1160	590	390	----	689
9a	.7335	.246	4.41	.20	48.3	52.6	570	.047	46.02	12.27	55	4.60	286	1790	1760	1070	740	500	72.1	737
9b	1.0240	.290	3.70	.20	42.3	49.8	559	.035	40.70	12.27	15	4.40	324	2170	2130	1240	----	---	66.7	653
10a	.3802	.147	5.02	.30	47.8	63.1	568	.076	44.16	12.25	15	3.02	80	880	1150	810	620	390	69.1	709
10b	.4284	.164	4.97	.29	49.3	60.3	584	.074	45.75	12.25	55	3.06	90	930	1190	820	620	400	71.4	722
10c	.5041	.192	4.97	.29	49.8	56.0	549	.041	47.78	12.25	20	2.96	148	1430	1380	720	510	380	----	759
11a	.4945	.172	4.49	.29	47.2	62.0	633	.066	44.03	12.23	20	2.95	134	1460	1490	920	650	---	68.1	692
11b	.6232	.215	4.46	.29	49.2	57.8	619	.062	46.22	12.23	20	2.84	162	1565	1600	940	610	---	66.5	730
[c]12	.6694	.219	4.18	.32	47.5	50.0	545	.057	44.77	12.23	35	2.78	183	1630	1700	900	600	---	----	725
13a	.7865	.242	3.97	.27	46.8	51.9	592	.066	43.70	12.23	30	3.24	238	2010	1850	1060	830	600	66.6	701
13b	.6372	.194	3.93	.27	44.3	53.4	583	.073	41.10	12.23	15	5.07	243	1700	1730	1020	800	570	66.4	655
13c	.5742	.194	4.40	.26	47.5	53.7	569	.065	44.43	12.23	15	4.39	191	1530	1690	980	800	560	68.2	698
14a	.8580	.261	3.91	.28	47.3	49.0	571	.058	44.55	12.23	30	2.70	180	1790	1880	1380	1040	760	71.9	717
14b	.5334	.190	4.65	.27	49.3	54.5	565	.064	46.15	12.23	22	2.01	153	1700	1800	1390	1120	770	75.2	742

[a]Runs with same number indicate consecutive data without engine shutdown.

[b]Includes estimated heat losses to fuel-injector cooling water and nozzle-wall surfaces between entry and throat.

[c]Preceded by unreported data at low combustion temperature that resulted in plugging of many nozzle pressure taps.

TABLE III. - NOZZLE PRESSURE-RATIO[a] DATA FOR NOZZLE OF 8-INCH-DIAMETER COMBUSTOR

Station \ Run[b]	[c]7	9a	9b	10a	10b	10c	11a	11b	[c]12	13a	13b	13c	14a	14b
5	0.835	0.832	0.832	0.828	0.829	0.832	0.832	0.832	0.829	0.830	0.831	0.832	0.831	0.830
6	-----	.730	.731	.728	.730	-----	.738	.738	-----	.729	.728	.730	.729	.729
7	-----	.613	.612	.597	.586	-----	.613	.615	-----	.608	.611	.607	.608	.608
8	-----	.515	.517	.491	.507	.519	.520	.518	-----	.511	.515	.506	.514	.515
9	-----	.451	.452	.431	.438	-----	.449	.455	-----	.445	.450	.445	.449	.448
10	-----	.366	.364	.348	.333	-----	.362	.346	-----	.356	.360	.346	.358	.361
11	-----	.274	.291	.266	.264	-----	.275	.262	-----	.273	.282	.276	.273	.275
12	-----	.200	.214	.196	.196	-----	.191	.182	-----	.189	.202	.195	.204	.203
13	-----	.110	.124	.108	.112	-----	.103	.098	-----	.099	.112	.104	.108	.102
14	-----	.082	.093	.089	.091	-----	.069	.068	-----	.073	.086	.079	.082	.080
Base	.079	.074	.084	.066	.066	.072	.076	.072	.074	.065	.070	.066	.087	.090
Plenum	.102	.078	.085	.067	.065	.074	.074	.077	.081	.080	.089	.089	.097	.098

[a]Pressure ratio is nozzle static pressure divided by combustor-exit stagnation pressure.

[b]Runs with same number indicate consecutive data without engine shutdown.

[c]Preceded by unreported data at low combustion temperature that resulted in plugging of many nozzle pressure taps.

CONFIDENTIAL

TABLE IV. - PERFORMANCE DATA FOR NOZZLE OF 8-INCH-DIAMETER COMBUSTOR

Run	Equivalence ratio, φ	Corrected combustor air temp., $T_{3,corr}$, °F	Corrected equivalence ratio, φ_{corr}	Static temp. at nozzle throat, t_8, °R	Ratio of specific heats, γ_8	Fluid constant, R_8	Stagnation temp., T_4, °R	Combustion efficiency, η_c, %	Boric oxide condensed at nozzle throat, %	Air specific impulse, S_a, sec	Nozzle-exit stream thrust computed from press. data, F_{15}, lb	Air specific stream thrust at exit, F_{15}/w_a, sec (a)	Divergence efficiency, η_w, % (b)	Divergence efficiency ratio (c)	Ratio of nozzle-exit stream thrust, $\frac{F_{15}}{F_{15,bb}}$
7	0.6280	-1	0.628	3022	1.261	52.38	3421	d_{97}	33	147.7	-----	-----	----	----	-----
9a	.7335	-148	.715	3133	1.260	52.75	3544	96	d_0	151.9	768.1	166.5	74.0	0.97	1.042
9b	1.0240	-247	.989	3302	1.246	52.44	3708	84	d_0	158.4	681.3	174.4	76.6	1.01	1.043
10a	.3802	82	.392	2305	1.282	52.21	2631	96	d_{100}	126.5	737.4	138.6	75.5	1.00	1.040
10b	.4284	78	.440	2508	1.274	52.05	2853	96	d_{100}	132.2	763.1	144.9	74.8	.98	1.057
10c	.5041	14	.506	2717	1.265	51.80	3080	95	d_{100}	137.9	-----	-----	----	----	-----
11a	.4945	91	.507	2780	1.265	51.83	3156	97	d_{100}	139.5	731.7	152.8	73.5	.97	1.057
11b	.6232	64	.632	3036	1.256	52.28	3419	d_{97}	36	147.5	765.1	160.9	70.2	.92	1.048
12	.6694	-83	.658	3146	1.256	52.12	3548	d_{97}	42	151.6	-----	-----	----	----	-----
13a	.7865	-101	.772	3287	1.250	52.66	3700	98	d_0	155.9	723.8	170.4	71.7	.94	1.032
13b	.6372	-118	.620	3085	1.256	51.88	3479	d_{97}	63	148.3	685.2	163.0	76.5	1.01	1.046
13c	.5742	-61	.565	2950	1.260	51.90	3336	d_{97}	74	144.5	737.5	158.1	72.8	.96	1.057
14a	.8580	-68	.848	3477	1.250	52.60	3918	97	d_{100}	161.1	742.8	177.0	75.8	1.00	1.036
14b	.5334	-24	.530	2882	1.260	51.70	3255	97	d_{100}	142.1	771.8	156.4	77.1	1.01	1.040

[redacted]

[a]Stream thrust computed from pressure data.

[b]$\eta_w = \left[\left(\sum pA \text{ for HEF-2}\right)100\right] / \left[\sum pA \text{ for one-dimensional isentropic flow of a perfect gas at constant } \gamma\right]$.

[c]$(\eta_w \text{ HEF-2})/(\eta_w \text{ warmup fuel})$.

[d]Assumed.

CONFIDENTIAL

TABLE V. - PRIMARY AND PERFORMANCE DATA FOR NOZZLE OF 28-INCH-DIAMETER AFTERBURNER

Run	Primary-burner equivalence ratio, φ	Corrected total equivalence ratio, φ_{corr}	JEF-2 flow, w_f, lb/sec	Primary-air flow, w_a, lb/sec	Atomizing-air flow, lb/sec	Corrected combustor air temp., $T_{3,corr}$, °R (a)	Nozzle-throat expansion coeff., C_k	Combustor cooling-air flow, lb/sec	Heat rejected to combustor coolant, q, Btu/sec	Exhaust-gas specific-heat ratio, γ	Primary-air temp., T_1, °R	Air specific impulse, S_a, sec	Stagnation temp., T_4, °R	Boric oxide condensed at nozzle throat, %	Combustion efficiency, η_c, %	Nozzle-exit wall temp., °R	Exhaust-nozzle inlet total press., P_4, lb/sq in.	Nozzle-exit plenum press., lb/sq in.
86	0.2215	0.4782	0.697	32.95	1.58	796	1.0163	13.09	740	1.27	885	141.1	3147	58	[b]100	1539	34.0	6.4
87	.2213	.4918	.705	33.34	1.57	788	1.0173	12.97	791	1.27	883	142.3	3194	55	[b]100	1592	34.6	6.5
88	.2217	.5860	.896	31.23	1.56	769	1.0196	12.14	886	1.26	882	150.1	3484	3	[b]100	1709	34.2	7.3
95	.2157	.5173	.772	32.57	1.40	718	1.0149	15.50	1418	1.27	892	144.3	3269	49	[b]100	1461	34.2	8.9
96	.2206	.6183	.965	30.36	1.37	712	1.0167	17.80	1331	1.26	887	153.0	3598	[b]0	101.3	1558	33.8	10.4
97	.2096	.6456	1.030	30.08	1.42	757	1.0154	14.05	1018	1.26	892	153.7	3618	[b]0	98.3	1489	33.8	6.2
98	.2189	.6198	.936	29.81	1.36	756	1.0151	14.16	970	1.26	895	151.9	3552	[b]0	99.3	1473	33.8	6.1
106	.1894	.5837	.927	31.52	1.32	877	1.0138	28.40	1108	1.25	1018	149.9	3513	24	[b]100	1405	34.4	8.1
107	.1940	.6787	1.082	29.35	1.40	844	1.0146	27.96	1223	1.25	1010	157.6	3789	[b]0	99.9	1447	33.9	8.5
108	.1924	.7041	1.134	28.88	1.32	813	1.0162	22.14	1329	1.25	997	160.0	3889	[b]0	99.4	1530	33.8	8.2
109	.2031	.7201	1.210	29.16	1.36	779	1.0153	30.21	1518	1.25	987	160.4	3883	[b]0	94.3	1476	34.2	8.5
117	.2078	.5264	.770	32.07	1.36	851	1.0121	15.84	1196	1.27	1000	145.8	3342	58	[b]100	1312	34.1	7.7
118	.2031	.5323	.768	31.46	1.32	884	1.0126	15.68	913	1.27	1000	145.8	3344	49	[b]100	1342	33.5	7.7
119	.2047	.5086	.722	32.23	1.37	812	1.0122	15.76	867	1.26	999	144.3	3282	70	[b]100	1320	33.9	7.7
120	.2049	.4933	.691	32.19	1.39	876	1.0116	15.63	992	1.26	999	142.8	3221	66	[b]100	1288	33.6	7.6
121	.1950	.4350	.590	34.12	1.38	910	1.0096	15.82	771	1.27	1000	138.1	3055	[b]100	102.2	1182	34.4	7.7
125	.1879	.3540	.438	36.16	1.57	974	1.0140	6.30	519	1.28	1031	129.3	2705	[b]100	103.3	1420	34.0	6.2
126	.1856	.3961	.500	34.88	1.60	976	1.0147	6.40	472	1.28	1030	132.5	2831	[b]100	99.9	1452	33.7	6.2
127	.1853	.4460	.618	33.83	1.49	964	1.0153	7.29	572	1.27	1031	137.6	3015	80	[b]100	1488	33.9	6.2
129	.1848	.4685	.692	33.02	1.59	894	1.0151	15.16	1080	1.27	1024	140.4	3120	86	[b]100	1424	33.9	7.2
130	.1864	.4973	.737	32.58	1.56	902	1.0157	15.45	996	1.26	1024	142.7	3219	66	[b]100	1500	34.0	7.2
138	.1980	.5281	.787	32.04	1.51	897	1.0163	16.09	929	1.26	1012	144.9	3306	27	[b]100	1536	33.9	7.9
140	.2013	.5556	.839	31.48	1.57	873	1.0161	16.09	1042	1.26	1004	146.9	3379	40	[b]100	1527	33.9	8.6
[c]99	.2193	.5058	-----	34.20	1.49	812	1.0152	14.06	752	1.28	881	-----	----	----	------	----	----	----
[c]85	.2110	.7867	-----	29.74	1.57	784	1.0178	12.41	726	1.26	899	-----	----	----	------	----	----	----

[a]Prior to any combustion.
[b]Assumed values.
[c]Primary burner only.

CONFIDENTIAL

CONFIDENTIAL

TABLE VI. - NOZZLE PRESSURE-RATIO DATA FOR REF-2 IN 28-INCH-DIAMETER AFTERBURNER

Run	Distance from nozzle entry, in.																						
	2	4	6	7	8	9	10	11	12	13	14	15	15.5	16	16.5	17	17.5	18	18.5	19	19.5	20	20.5	21
86	0.9902	0.9804	0.9679	0.9575	0.9465	0.9323	0.9189	0.8992	0.8751	0.8491	0.8188	0.7814	0.7567	0.7426	0.6908	0.6958	0.6720	0.6492	0.6293	0.6109	0.5906	0.5558	0.5309	0.5019
87	.9893	.9798	.9678	.9591	.9474	.9344	.9182	.8997	.8780	.8499	.8201	.7841	.7571	.7414	.7080	.6955	.6727	.6505	.6297	.6106	.5882	.5595	.5336	.5042
88	.9907	.9796	.9673	.9584	.9480	.9339	.9185	.8997	.8762	.8490	.8173	.7674	.7581	.7435	.7146	.6941	.6705	.6480	.6296	.6090	.5869	.5567	.5313	.5059
95	.9911	.9819	.9686	.9605	.9501	.9366	.9208	.9026	.8783	.8523	.8194	.7866	.7587	.7466	.7184	.6969	.6719	.6521	.6321	.6136	.5891	.5614	.5361	.5106
96	.9903	.9809	.9669	.9579	.9480	.9346	.9177	.9004	.8759	.8484	.8173	.7855	.7575	.7320	.7124	.6924	.6633	.6492	.6294	.6110	.5890	.5606	.5335	.5106
97	.9916	.9782	.9677	.9585	.9489	.9360	.9191	.9005	.8764	.8510	.8160	.7848	.7574	.7275	.7100	.6952	.6703	.6502	.6295	.6115	.5895	.5589	.5313	.5082
98	.9925	.9802	.9667	.9566	.9487	.9353	.9201	.8986	.8761	.8495	.8193	.7866	.7571	.7301	.7133	.6959	.6699	.6499	.6289	.6107	.5864	.5605	.5338	.5093
106	.9906	.9816	.9695	.9596	.9490	.9351	.9198	.9009	.8767	.8502	.8192	.7875	.7574	.7320	.7151	.6935	.6696	.6439	.6271	.6099	.5866	.5566	.5297	.5035
107	.9875	.9811	.9664	.9002	.9471	.9334	.9181	.9001	.8761	.8510	.8178	.7867	.7591	.7330	.7158	.6956	.6720	.6511	.6300	.6122	.5867	.5585	.5313	.5051
108	.9900	.9840	.9680	.9573	.9477	.9350	.9181	.8990	.8754	.8502	.8190	.7858	.7557	.7320	.7145	.6955	.6695	.6500	.6283	.6115	.5879	.5585	.5300	.5057
109	.9892	.9783	.9605	.9557	.9465	.9335	.9195	.8989	.8742	.8500	.8195	.7869	.7620	.7303	.7155	.6950	.6720	.6515	.6300	.6100	.5890	.5590	.5278	.5000
117	.9877	.9800	.9673	.9558	.9461	.9321	.9169	.8901	.8752	.8492	.8183	.7877	.7590	.7371	.7178	.6958	.6743	.6498	.6268	.6079	.5847	.5568	.5281	.5032
118	.9916	.9836	.9696	.9612	.9499	.9352	.9207	.9004	.8779	.8520	.8214	.7879	.7603	.7375	.7149	.6984	.6759	.6528	.6304	.6133	.5877	.5593	.5302	.5030
119	.9899	.9801	.9684	.9577	.9473	.9318	.9158	.8930	.8723	.8467	.8145	.7855	.7522	.7367	.7134	.6944	.6722	.6485	.6240	.6056	.5802	.5530	.5236	.4982
120	.9897	.9806	.9673	.9584	.9482	.9332	.9176	.8987	.8748	.8471	.8166	.7839	.7831	.7339	.7135	.6908	.6728	.6483	.6267	.6093	.5833	.5557	.5249	.5013
121	.9910	.9773	.9673	.9604	.9490	.9354	.9187	.8907	.8756	.8472	.8151	.7774	.7485	.7273	.7084	.6874	.6649	.6433	.6208	.6024	.5763	.5504	.5181	.4980
125	.9916	.9819	.9649	.9566	.9444	.9320	.9151	.8896	.8727	.8595	.8144	.7899	------	.7334	.7095	.6897	.6657	.6466	.6272	.6102	.5863	.5570	.5320	.5103
126	.9897	.9811	.9668	.9600	.9475	.9356	.9193	.8962	.8760	.8498	.8190	.7888	------	.7377	.7139	.6941	.6701	.6468	.6313	.6138	.5901	.5604	.5356	.5061
127	.9891	.9796	.9654	.9560	.9456	.9320	.9173	.8951	.8742	.8464	.8167	.7862	------	.7386	.7127	.6951	.6701	.6504	.6292	.6136	.5903	.5611	.5377	.5107
129	.9899	.9808	.9666	.9587	.9488	.9344	.9193	.8984	.8755	.8501	.8172	.7867	------	.7394	.7136	.6965	.6712	.6528	.6301	.6145	.5896	.5605	.5332	.5051
130	.9904	.9824	.9665	.9567	.9461	.9366	.9221	.8992	.8771	.8494	.8194	.7907	------	.7398	.7161	.6954	.6727	.6519	.6317	.6146	.5920	.5611	.5338	.5028
138	.9895	.9799	.9672	.9594	.9475	.9339	.9171	.9057	.8751	.8489	.8178	.7876	.7547	.7320	.7161	.6961	.6726	.6513	.6319	.6136	.5895	.5588	.5333	.5087
140	.9909	.9790	.9674	.9587	.9477	.9348	.9194	.9103	.8744	.8493	.8191	.7885	.7547	.7357	.7161	.6954	.6752	.6529	.6314	.6143	.5891	.5577	.5318	.5067
99	.9909	.9826	.9652	.9572	.9490	.9339	.9190	.8993	.8743	.8486	.8182	.7902	.7537	.7267	.7098	.6974	.6831	.6453	.6259	.6066	.5856	.5556	.5326	.5153
85	.9936	.9826	.9694	.9614	.9504	.9366	.9206	.9012	.8768	.8493	.8204	.7863	.7563	.7278	.7107	.6964	.6698	.6506	.6316	.6142	.5942	.5564	.5400	.5355

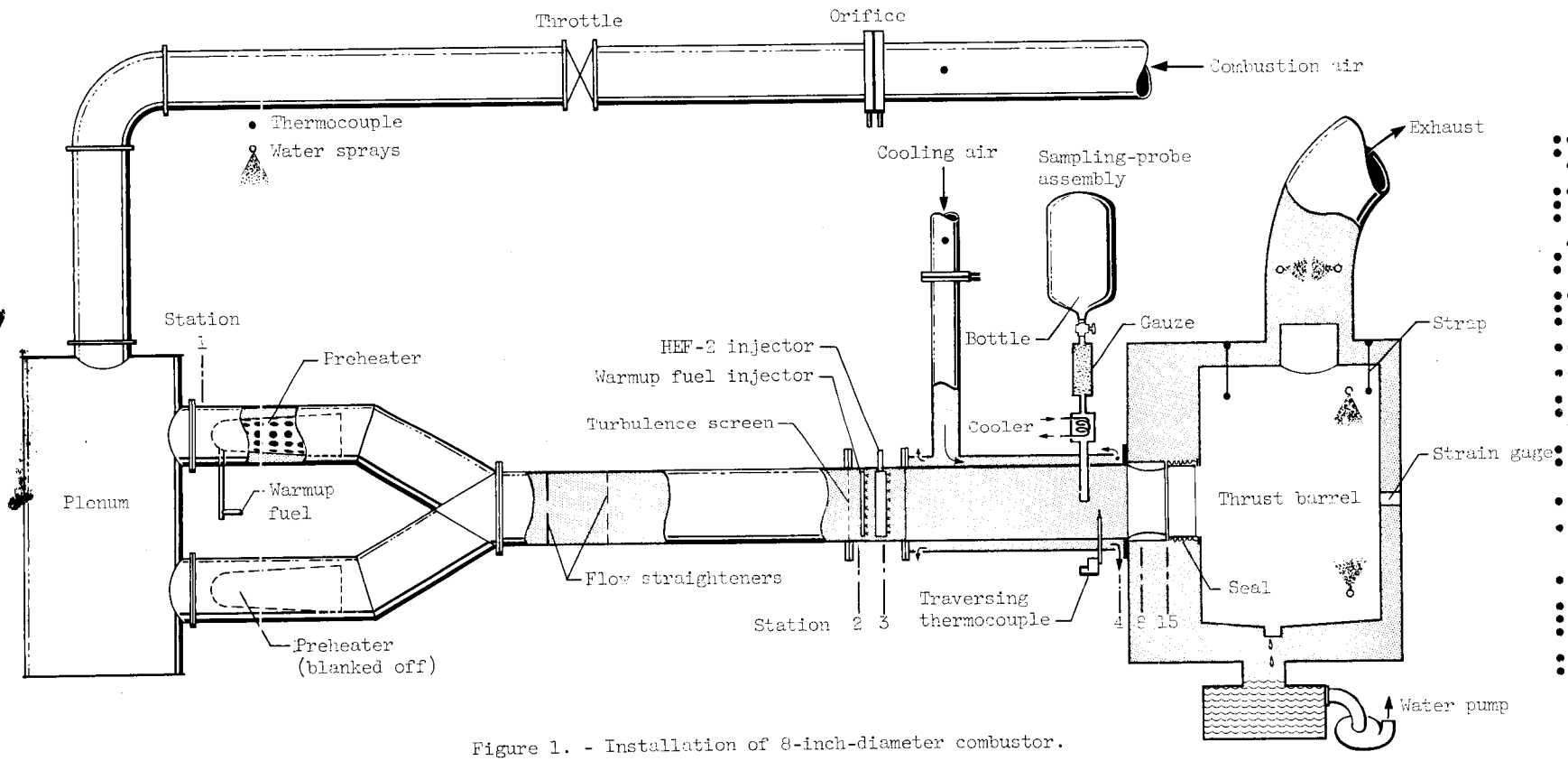

Figure 1. - Installation of 8-inch-diameter combustor.

CD-6913

CONFIDENTIAL

CONFIDENTIAL

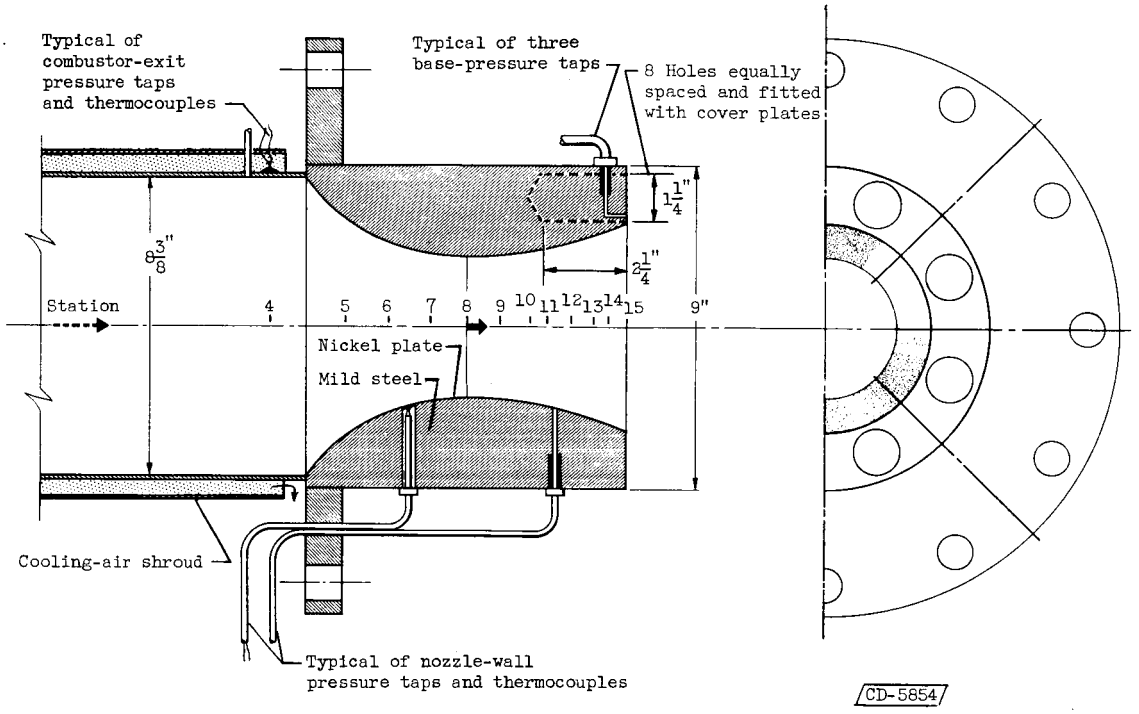

Station	Distance from throat, in.	A/A_8	Static-pressure taps	Thermocouples
4	6.00	4.4	4	4
Inlet	4.00	4.4	0	0
5	2.20	1.300	1	4
6	1.41	1.097	2	0
7	.70	1.012	2	0
[a]8	0	1.000	4	4
9	.48	1.012	2	0
10	1.00	1.050	2	0
11	1.52	1.131	4	4
12	2.12	1.269	2	0
13	2.79	1.519	2	0
14	3.01	1.630	4	4
15	3.10	1.680	0	0

[a]Nominal throat diam., 4 in.

Figure 2. - Diagram and dimensions of convergent-divergent nozzle for 8-inch-diameter combustor.

[redacted]AL

DECLASSIFIED
CONFIDENTIAL

E-796
CR-5 back

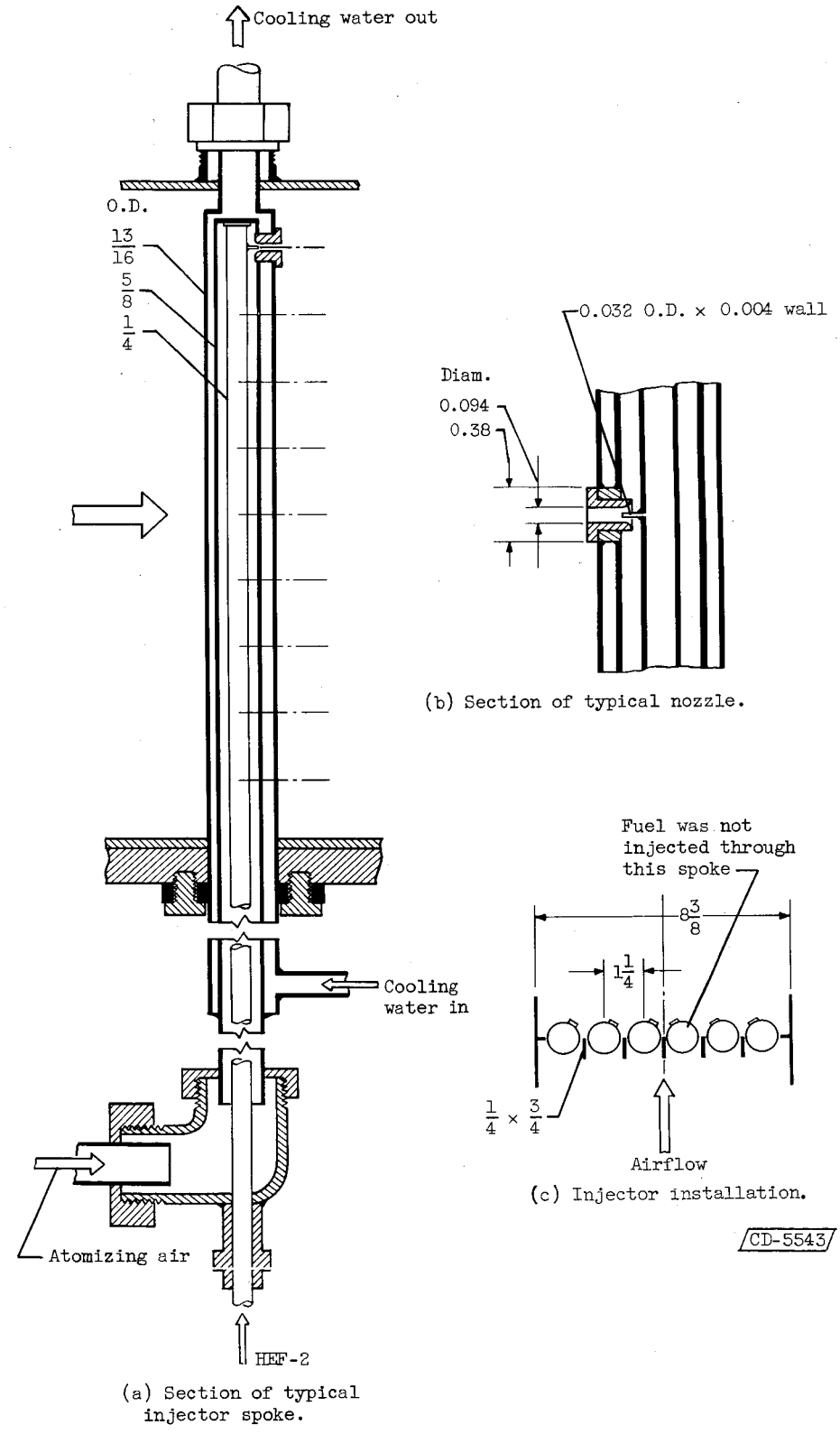

(a) Section of typical injector spoke.

(b) Section of typical nozzle.

(c) Injector installation.

Figure 3. - HEF-2 injector for 8-inch-diameter combustor (dimensions in inches).

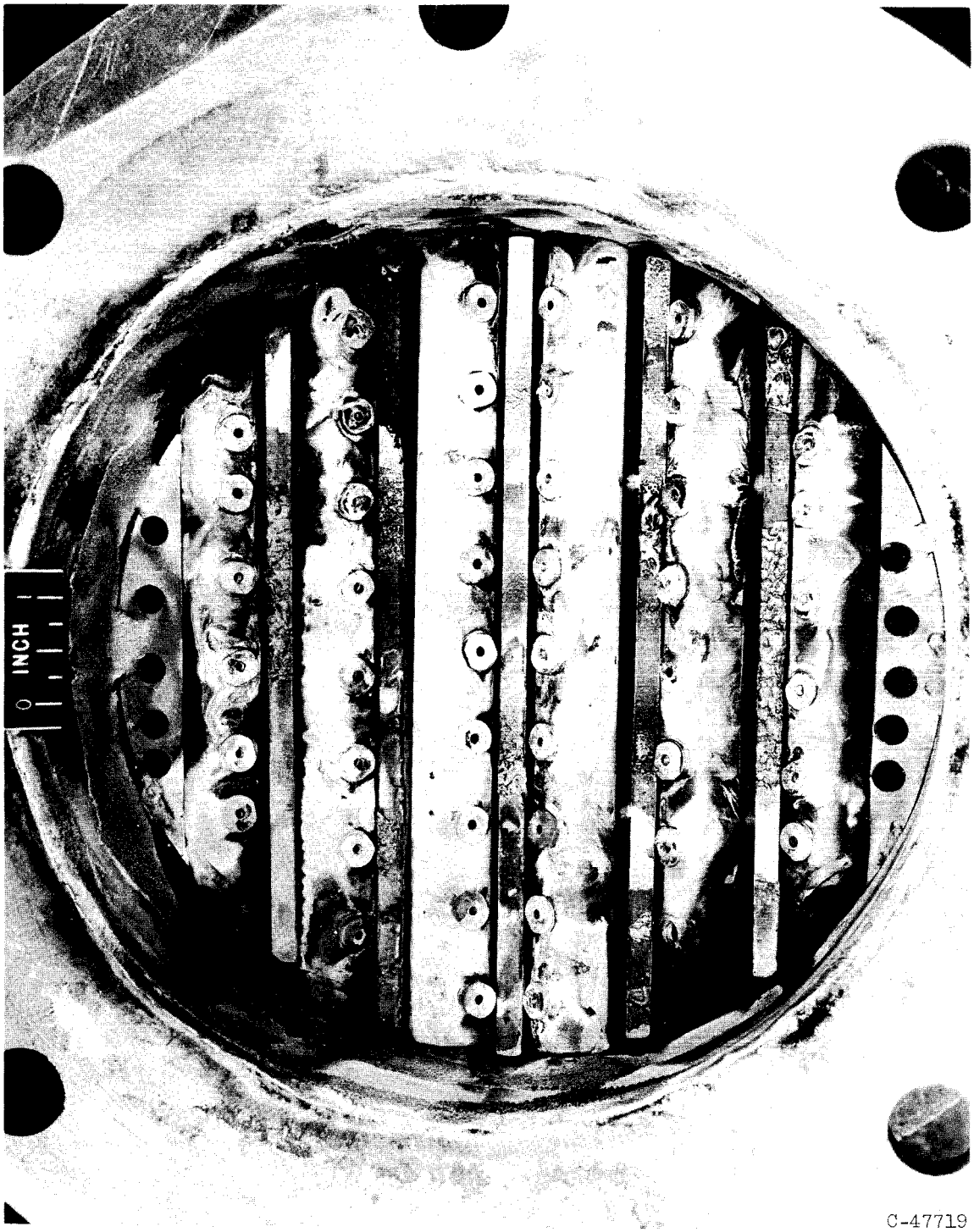

Figure 4. - HEF-2 injector for 8-inch-diameter combustor (view looking upstream).

DECLASSIFIED
CONFIDENTIAL

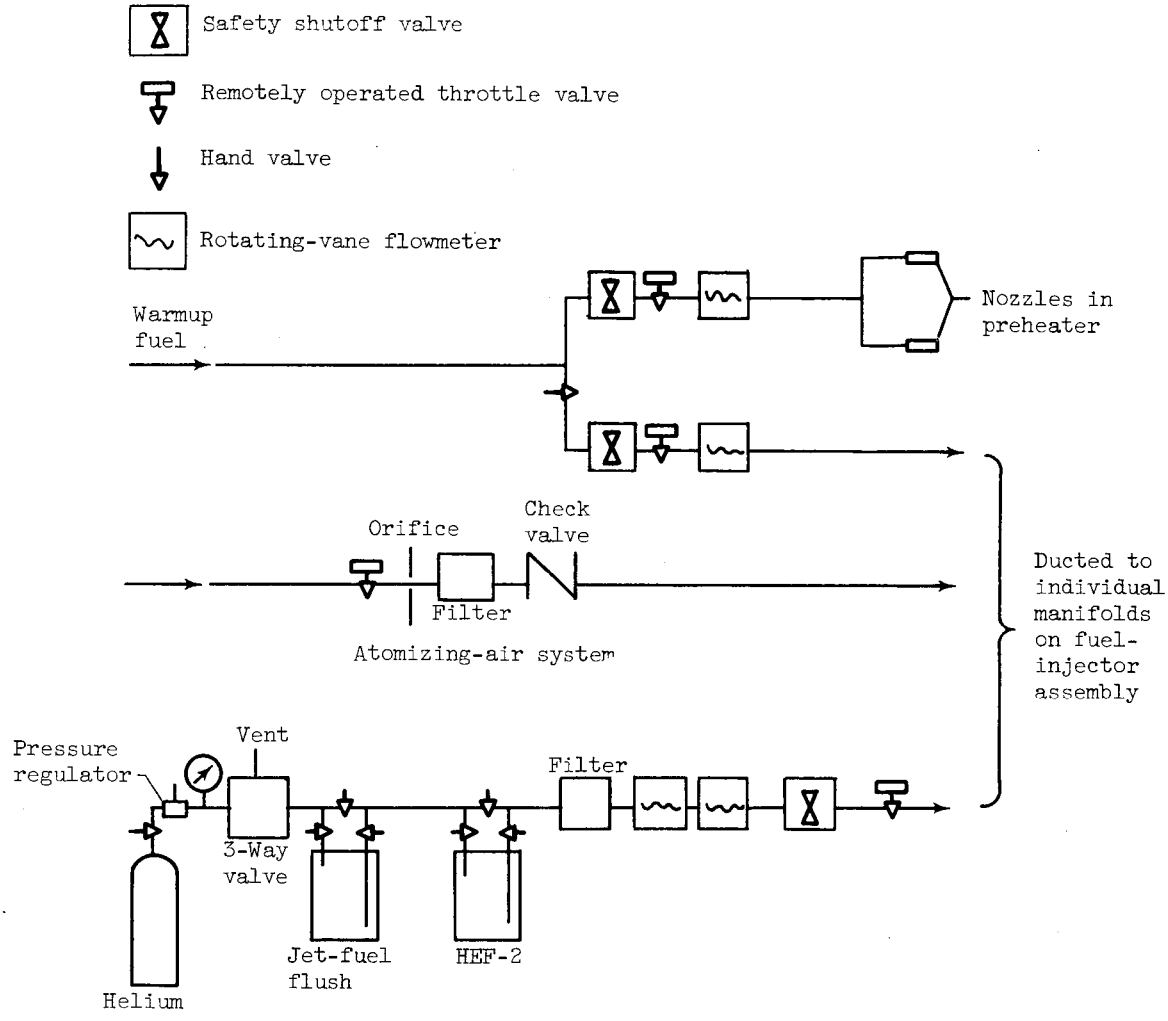

Figure 5. - Fuel systems for 8-inch-diameter combustor.

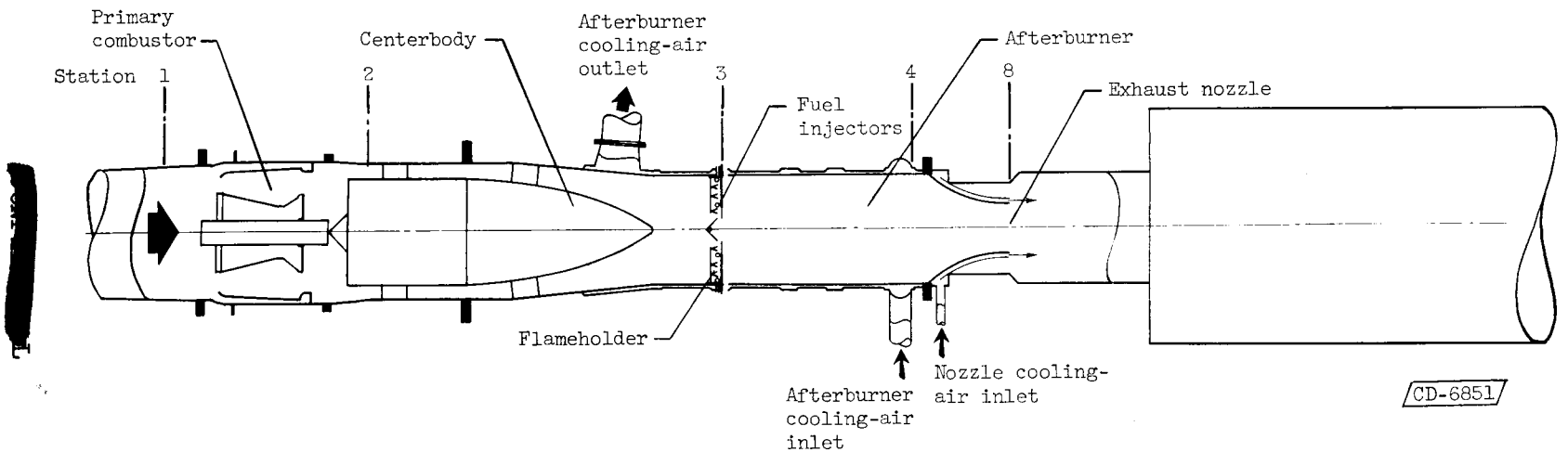

Figure 6. - Installation of 28-inch-diameter afterburner.

CONFIDENTIAL

DECLASSIFIED
CONFIDENTIAL

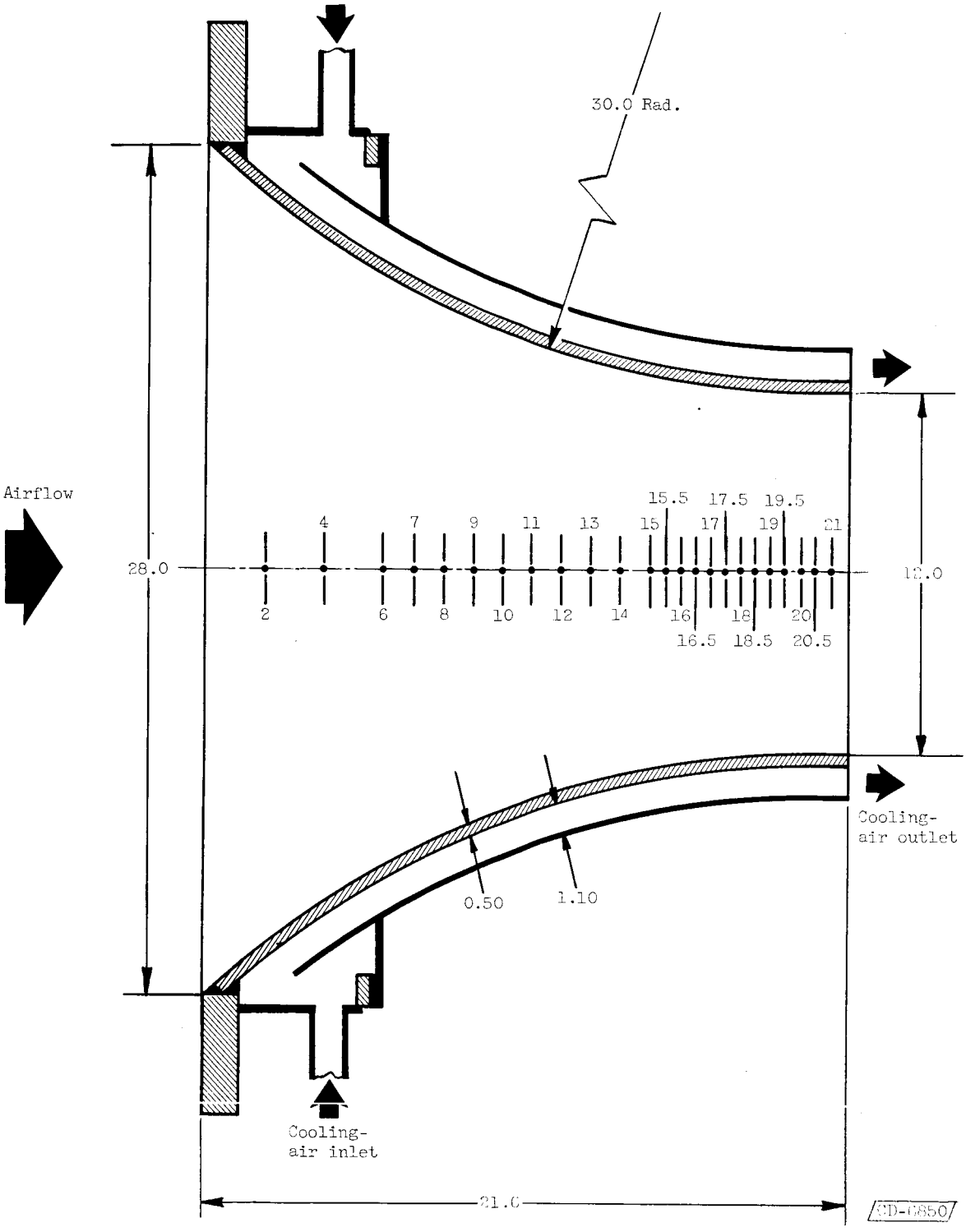

Figure 7. - Convergent exhaust nozzle for 28-inch-diameter afterburner (dimensions in inches).

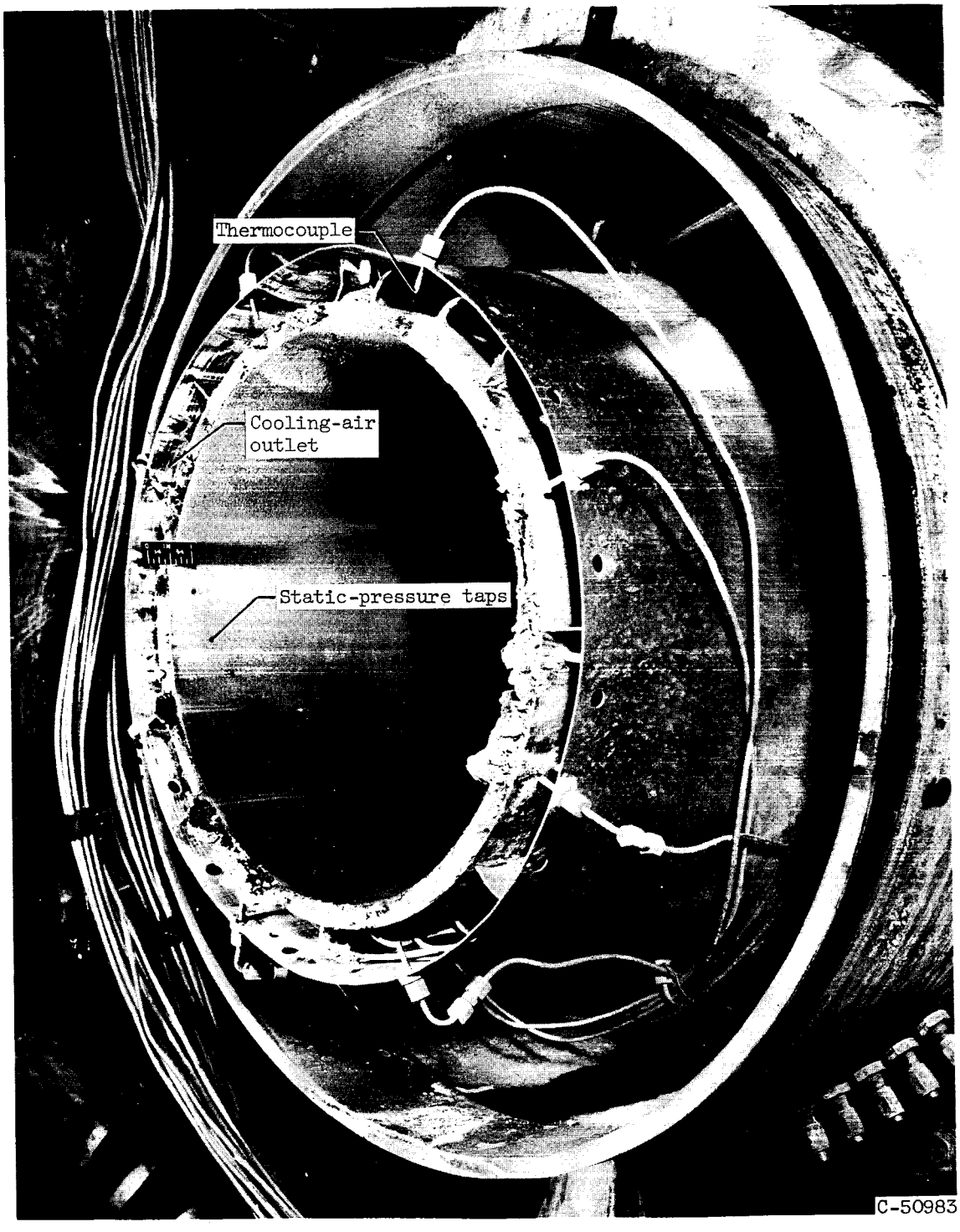

Figure 8. - Convergent exhaust nozzle for 28-inch-diameter afterburner.

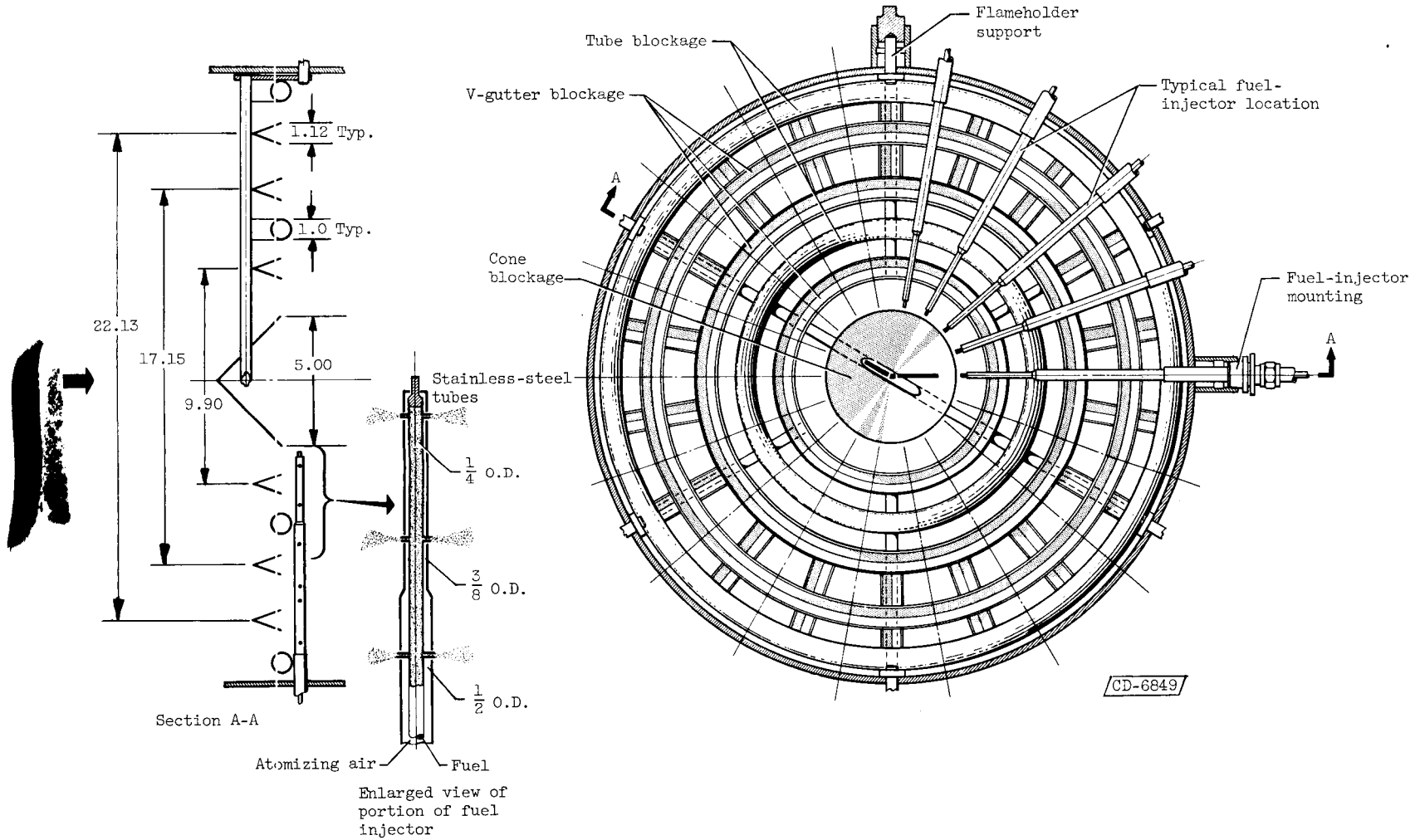

Figure 9. - Flameholder - fuel-injector configuration for 28-inch-diameter afterburner (dimensions in inches).

CONFIDENTIAL

CONFIDENTIAL

Figure 10. - Flameholder - fuel-injector configuration for 28-inch-diameter afterburner after several runs (looking upstream).

DECLASSIFIED

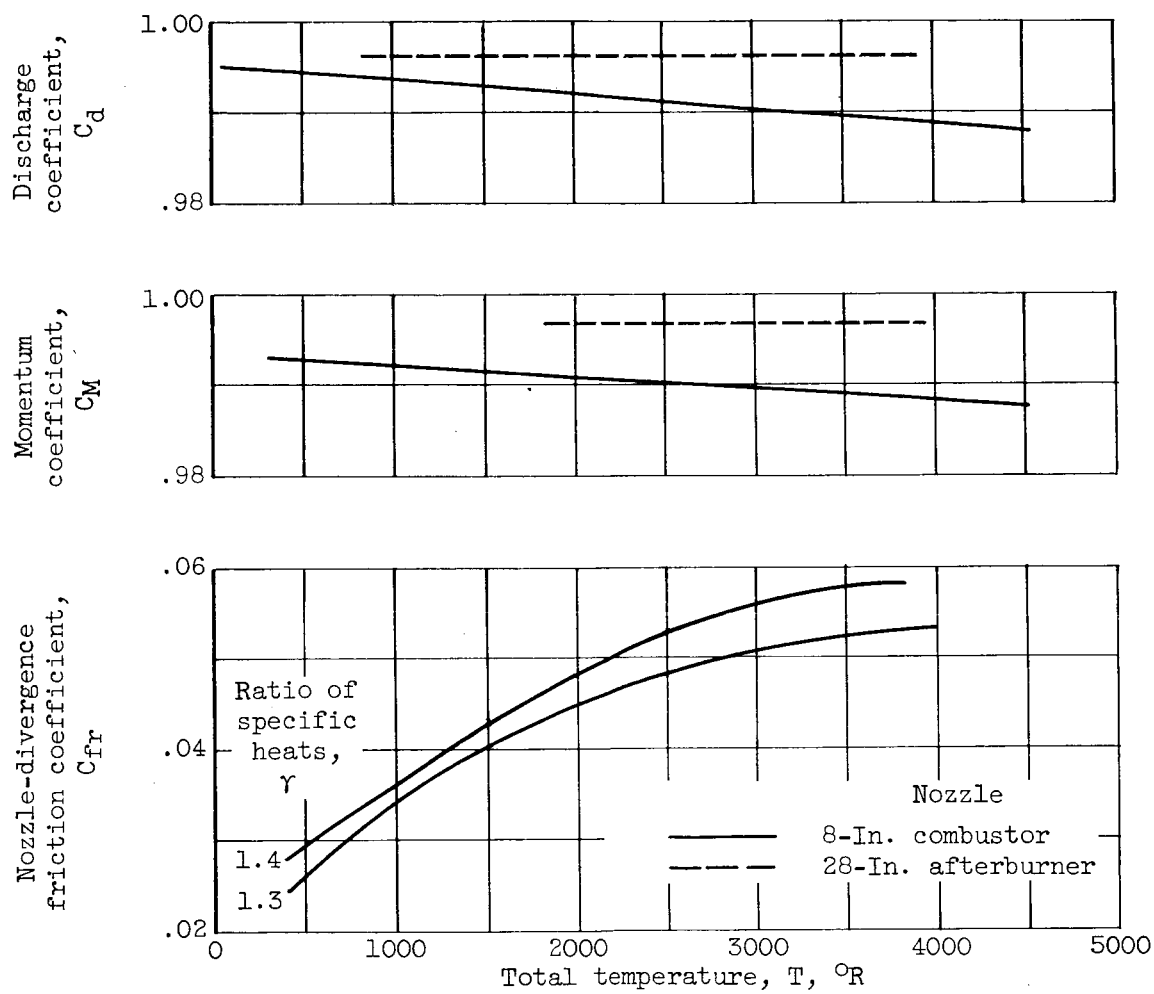

Figure 11. - Coefficients that express deviation from one-dimensional ideal flow in the nozzles.

CONFIDENTIAL

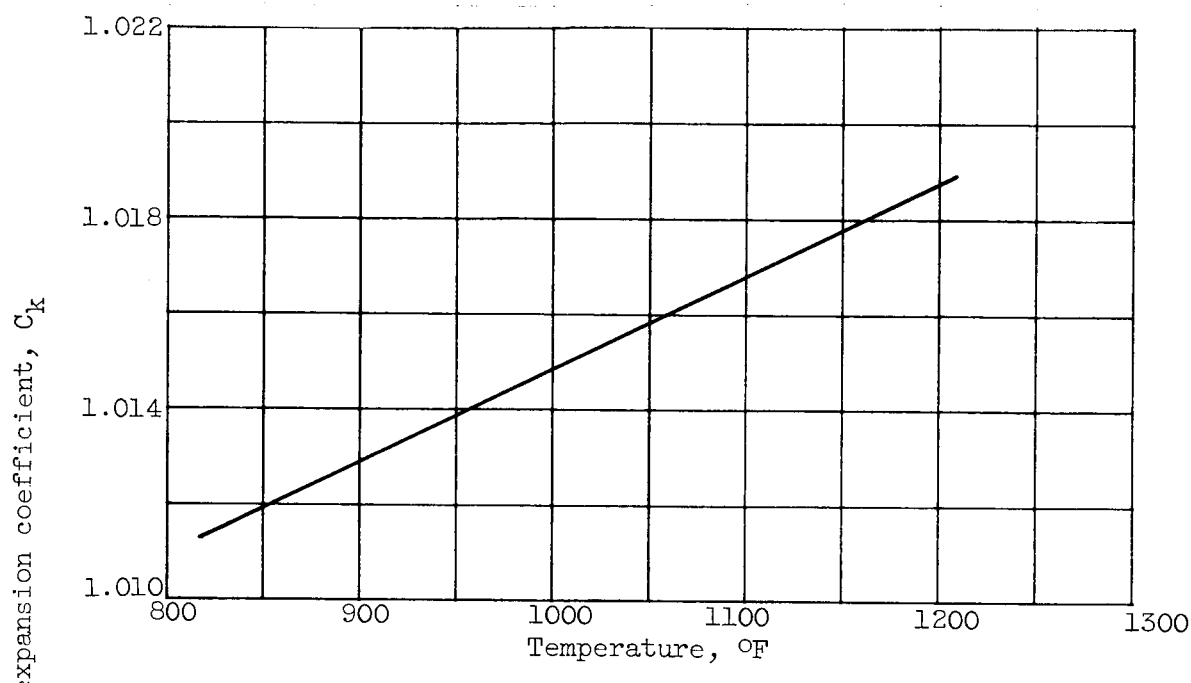

(a) 28-Inch-diameter afterburner nozzle.

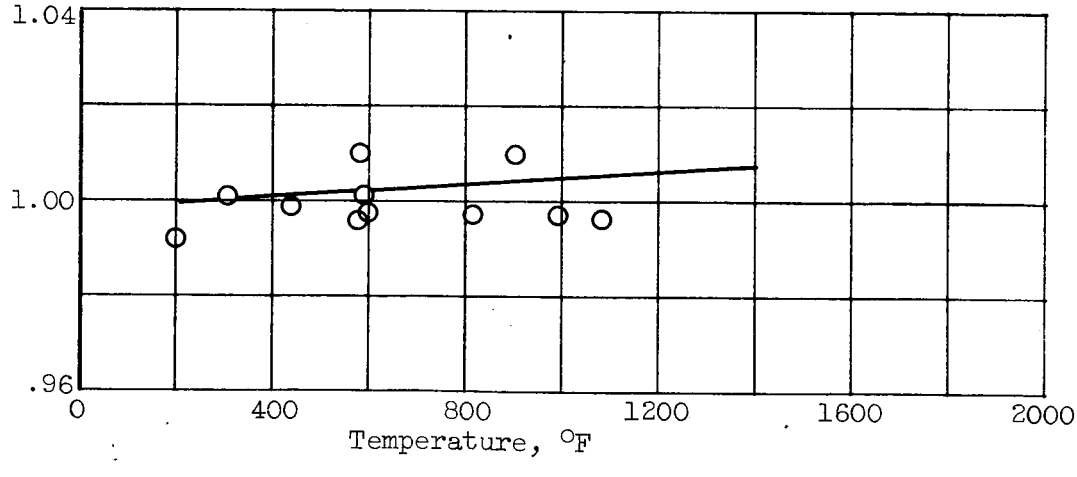

(b) 8-Inch-diameter combustor nozzle.

Figure 12. - Effect of wall temperature at nozzle throat on throat area for warmup-fuel products of combustion.

[redacted]L

DECLASSIFIED

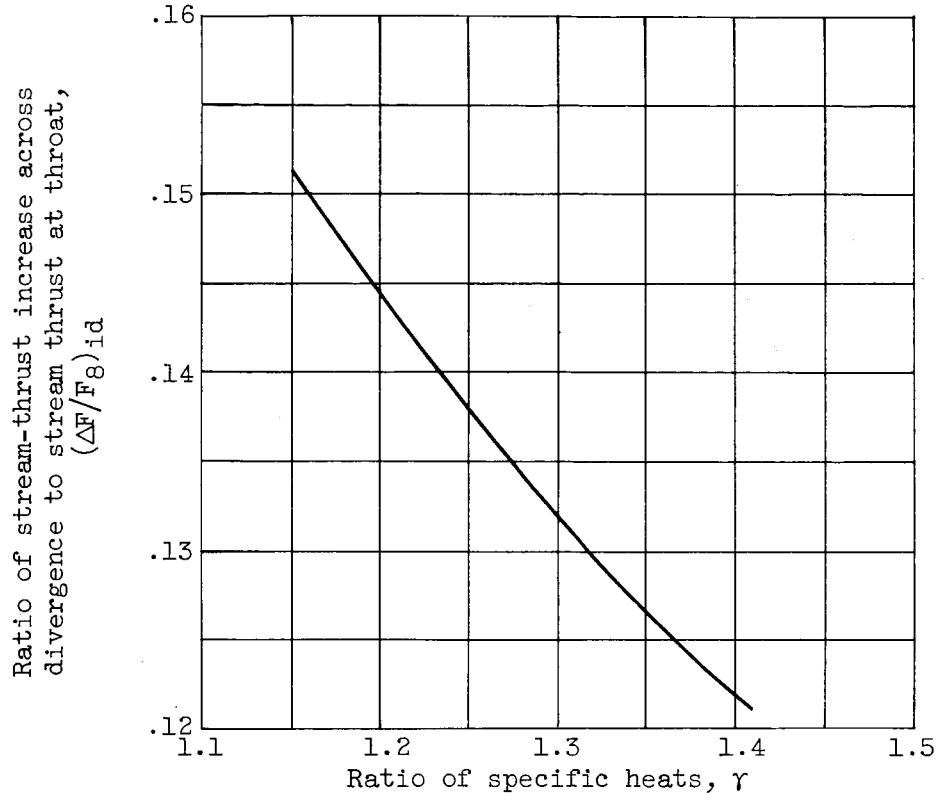

Figure 13. - Effect of ratio of specific heats on divergence stream thrust for ideal one-dimensional flow. Nozzle-exit- to throat-area ratio, 1.68; 8-inch-diameter combustor nozzle.

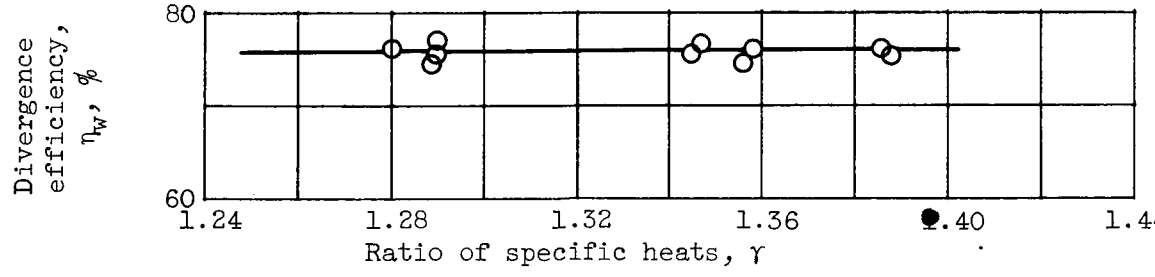

Figure 14. - Comparison of actual and ideal stream thrust produced in divergent portion of exhaust nozzle for warmup-fuel products of combustion for 8-inch-diameter combustor nozzle.

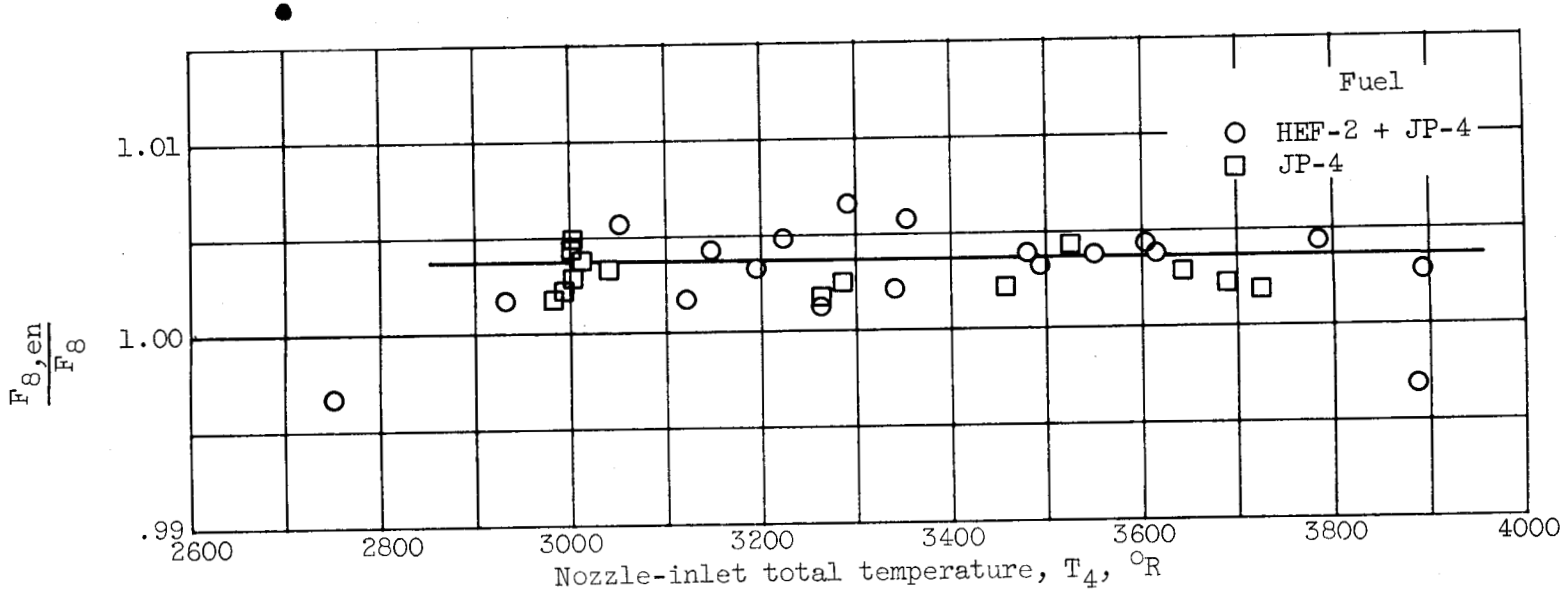

Figure 15. - Comparison of thrust computed from momentum envelope within 28-inch-diameter afterburner nozzle $F_{8,en}$ and from one-dimensional isentropic flow analysis F_8.

CONFIDENTIAL

DECLASSIFIED
CONFIDENTIAL

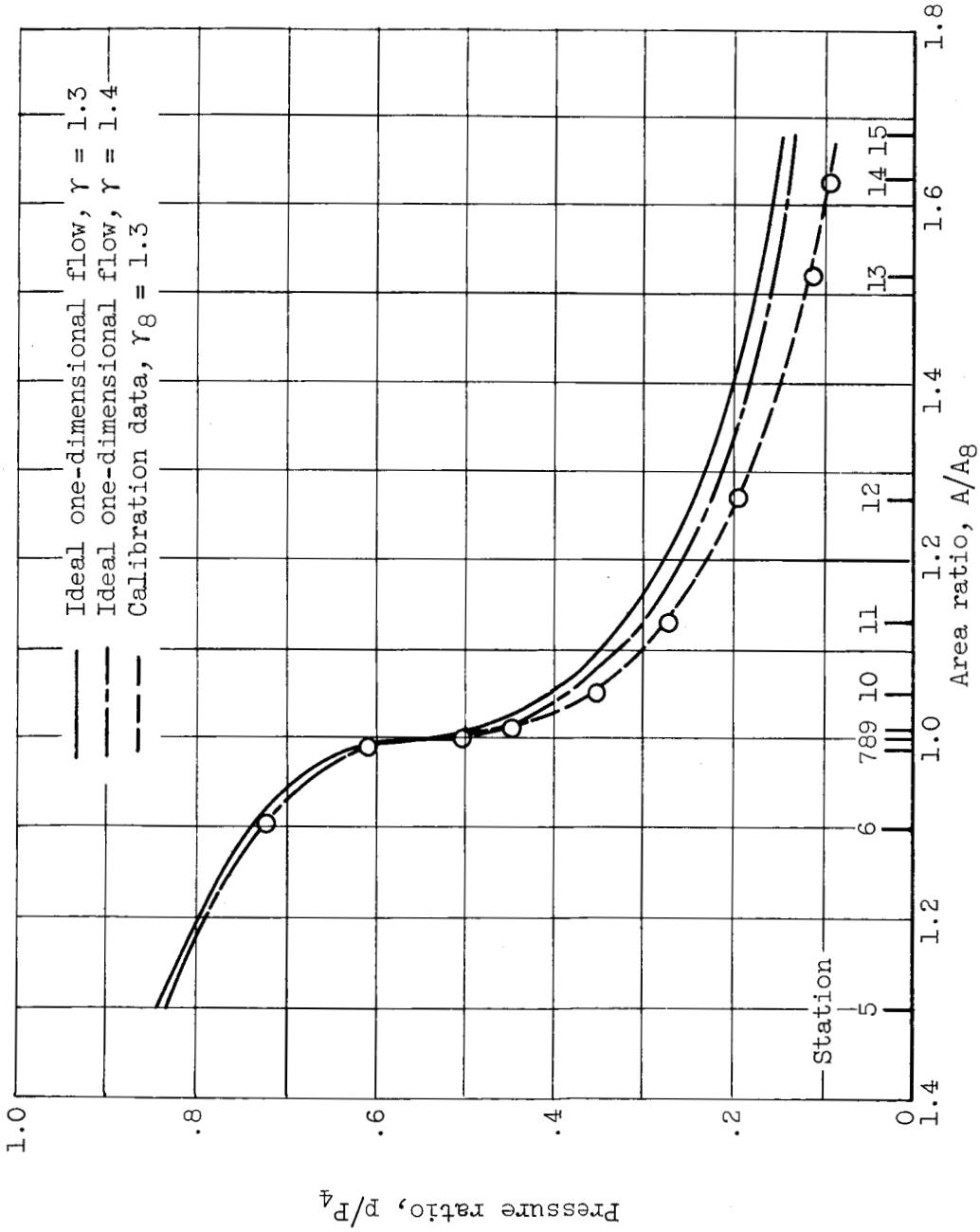

Figure 16. - Comparison of one-dimensional and measured three-dimensional flow in convergent-divergent nozzle.

E-796

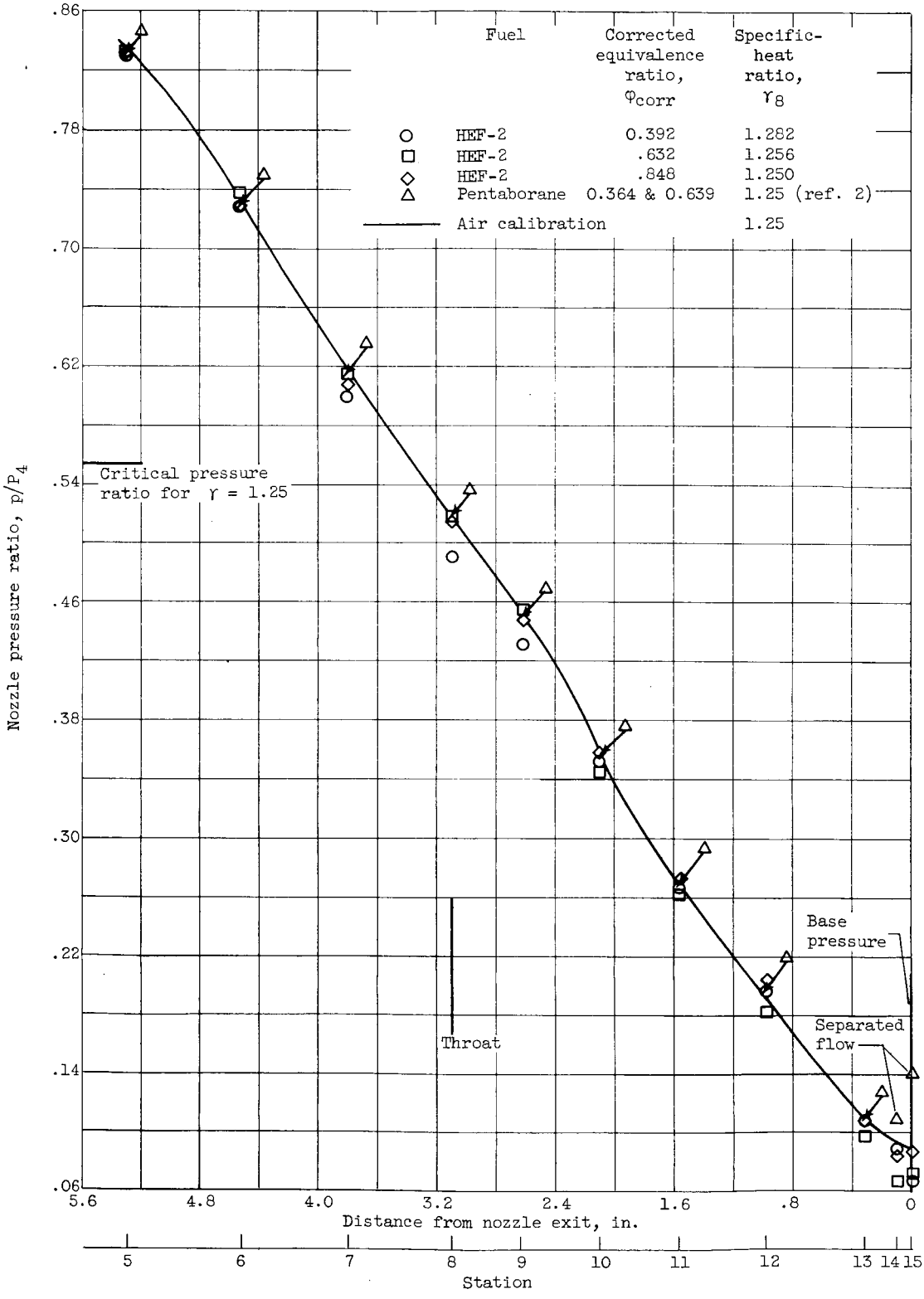

Figure 17. - Ratios of static to total pressure throughout 8-inch-diameter combustor convergent-divergent exhaust nozzle.

DECLASSIFIED

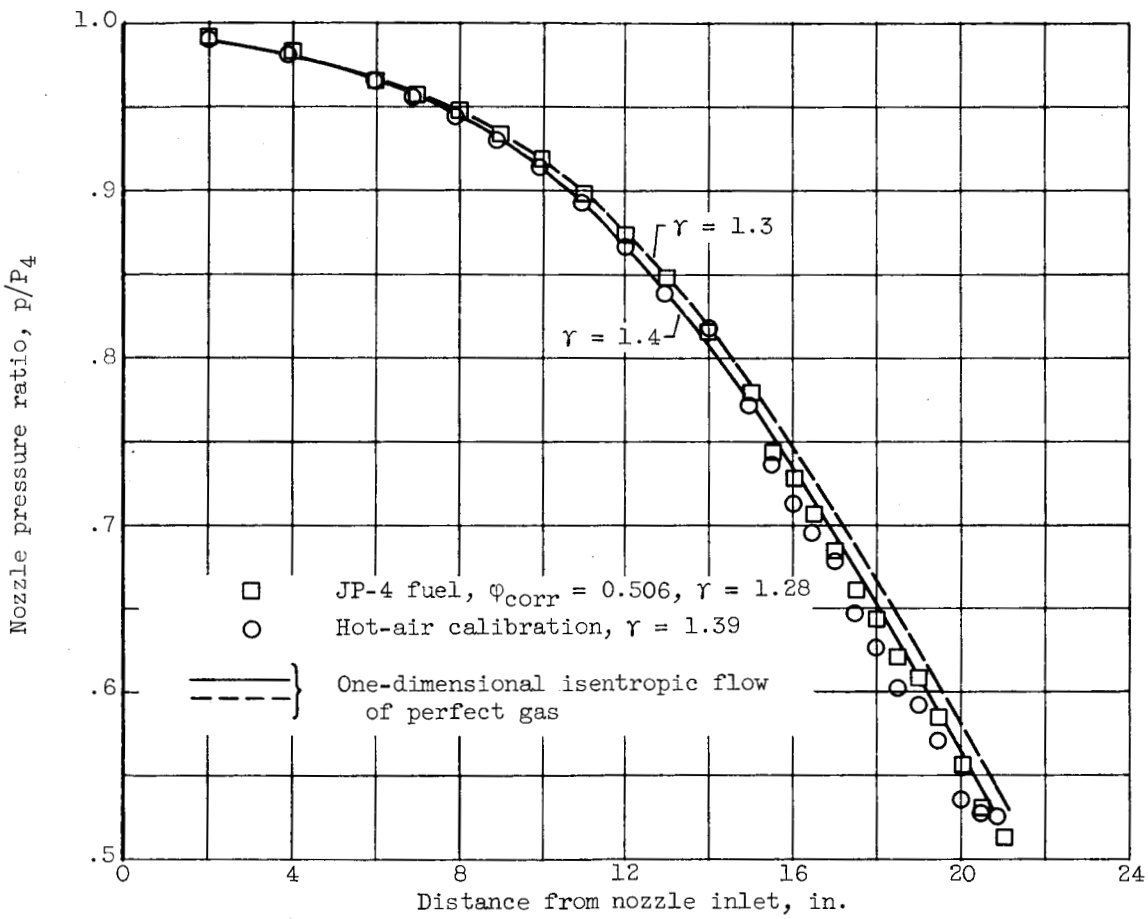

(a) Comparison of pressure ratios for ideal flow with hot-air calibration and with expansion of JP-4 combustion products.

Figure 18. - Ratios of static to total pressure throughout 28-inch-diameter afterburner convergent exhaust nozzle.

CONFIDENTIAL

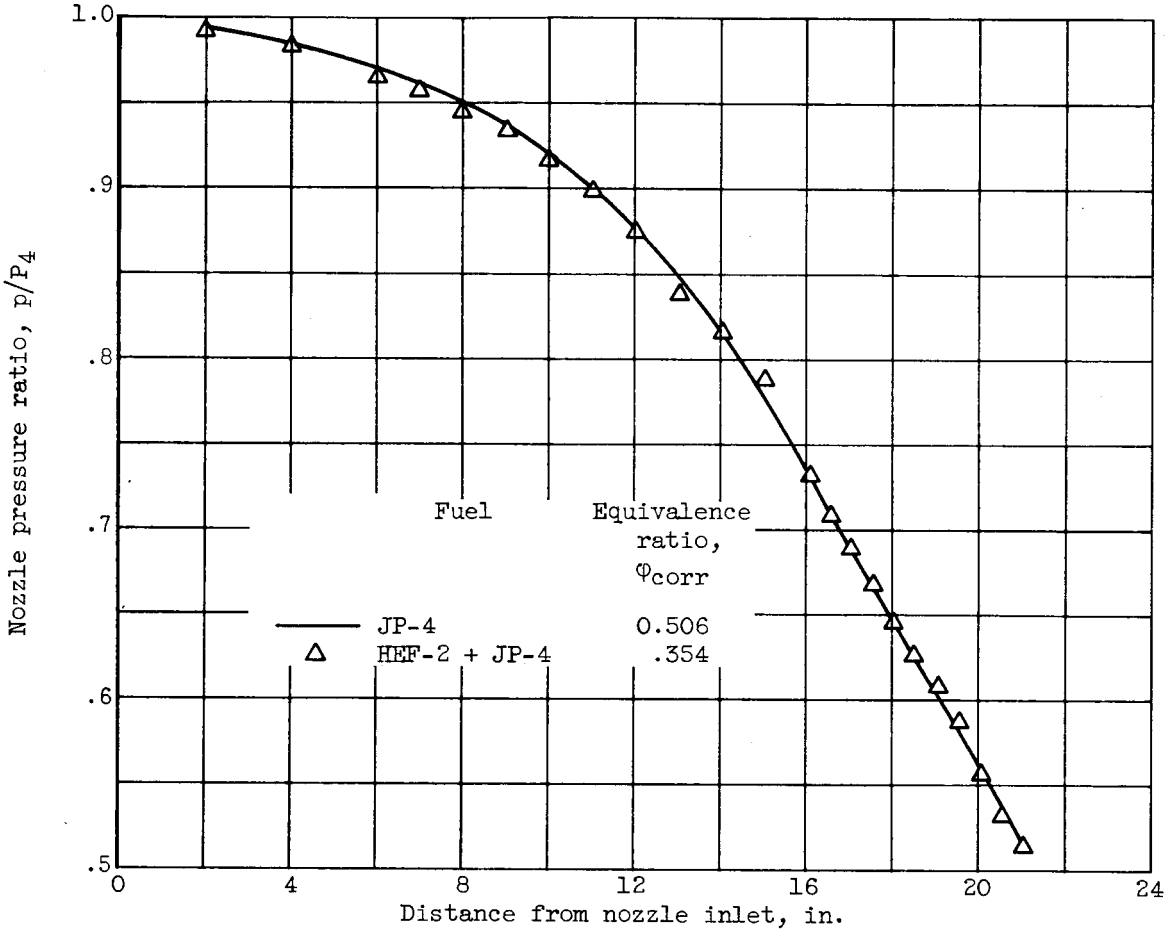

(b) Comparison of pressure ratios for "clean" combustion products of JP-4 with those of HEF-2 + JP-4 for γ of 1.28.

Figure 18. - Continued. Ratios of static to total pressure throughout 28-inch-diameter afterburner convergent exhaust nozzle.

DECLASSIFIED

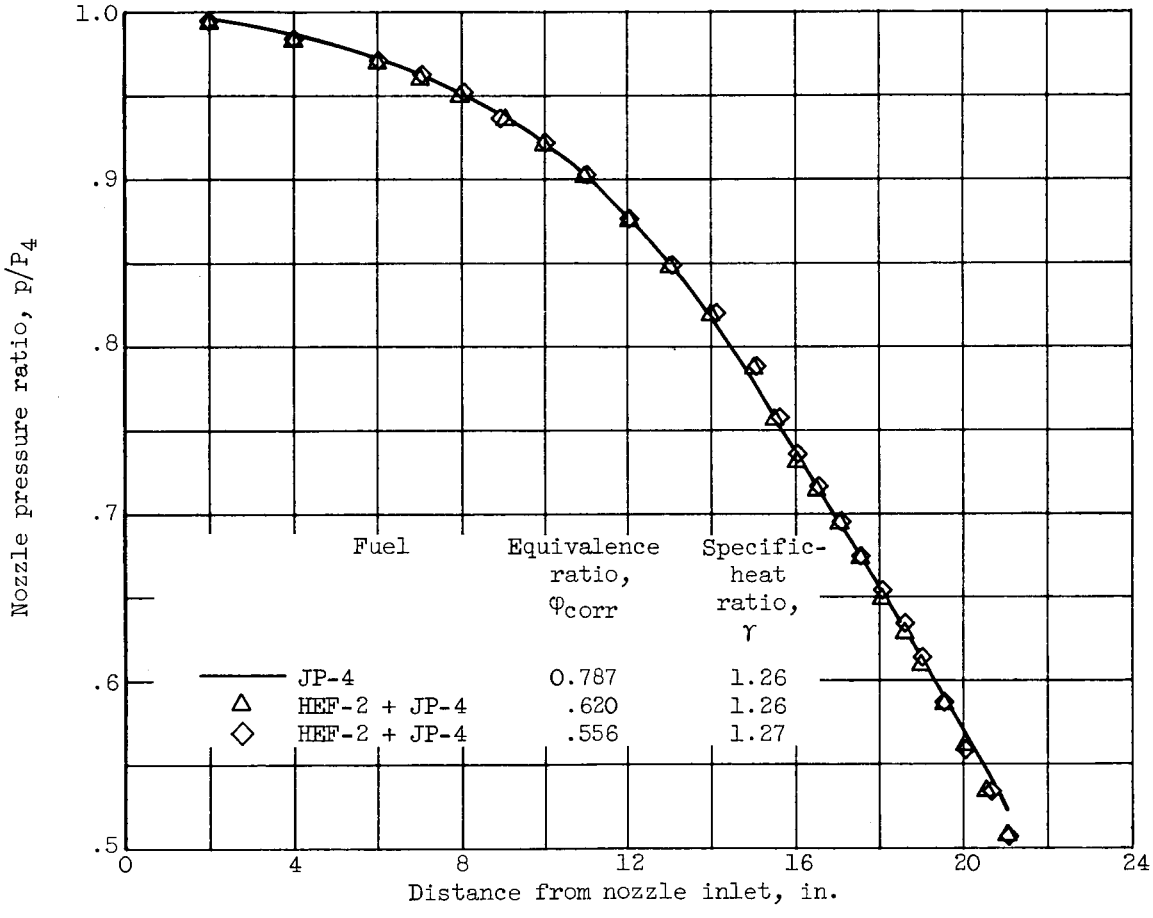

(c) Comparison of pressure ratios for "clean" combustion products of JP-4 with those of HEF-2 + JP-4 for γ of 1.26.

Figure 18. - Concluded. Ratios of static to total pressure throughout 28-inch-diameter afterburner convergent exhaust nozzle.

CONFIDENTIAL

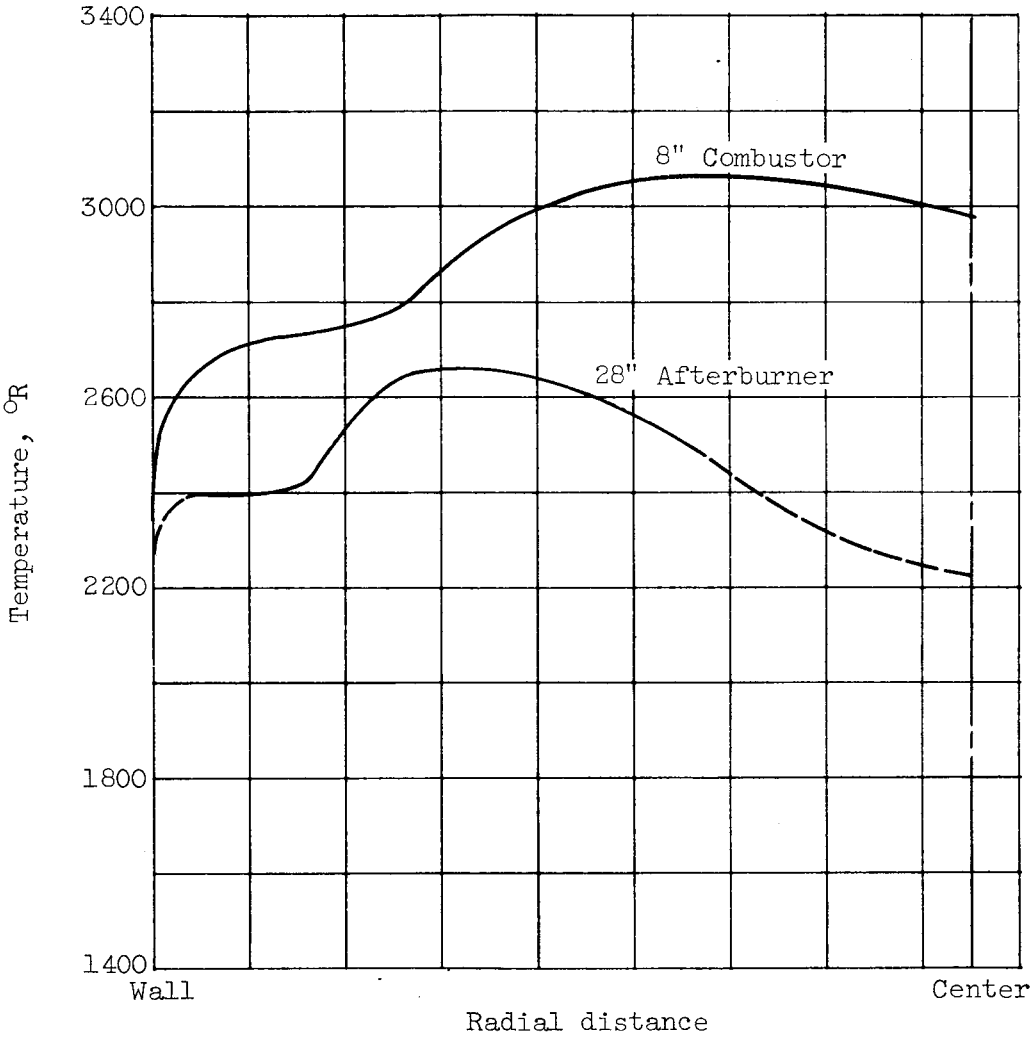

Figure 19. - Typical combustor-exit temperature profiles (station 4).

[redacted]

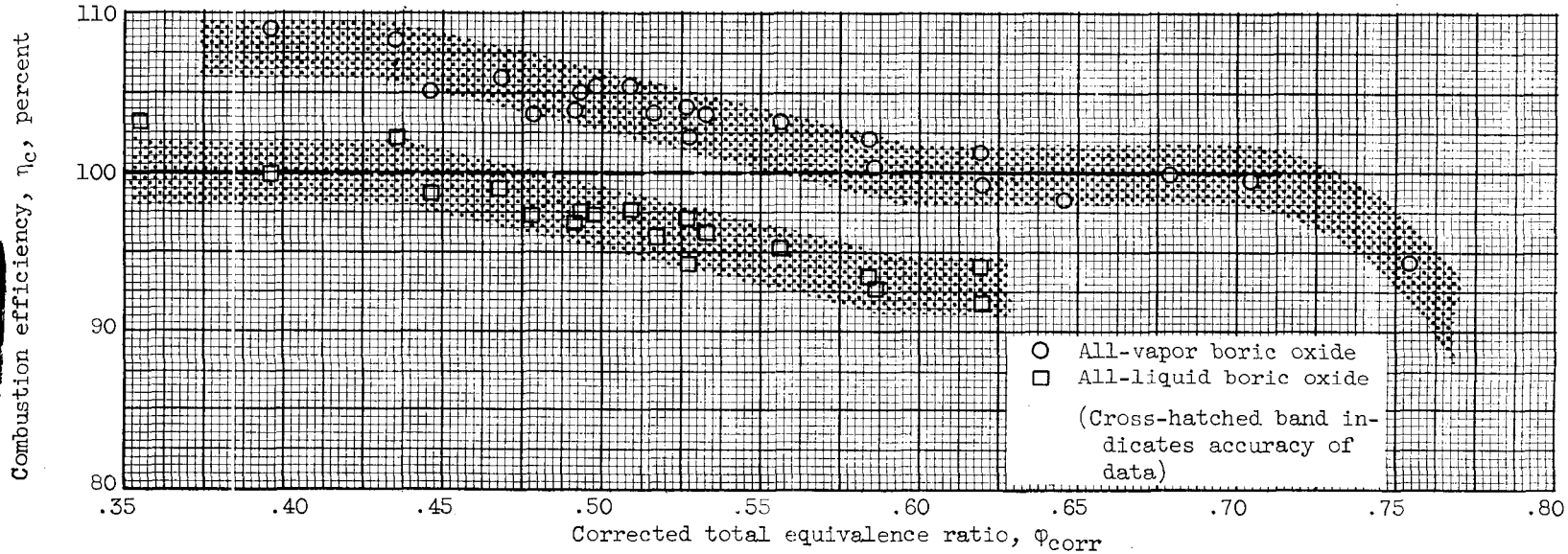

Figure 20. - Combustion efficiency for 28-inch-diameter afterburner. Primary-burner fuel, JP-4 at approximate equivalence ratio of 0.2; afterburner fuel, HEF-2; primary-burner-inlet air temperature, 844° R; combustor pressure, $2\frac{1}{2}$ atmospheres.

CONFIDENTIAL

CONFIDENTIAL

E-796

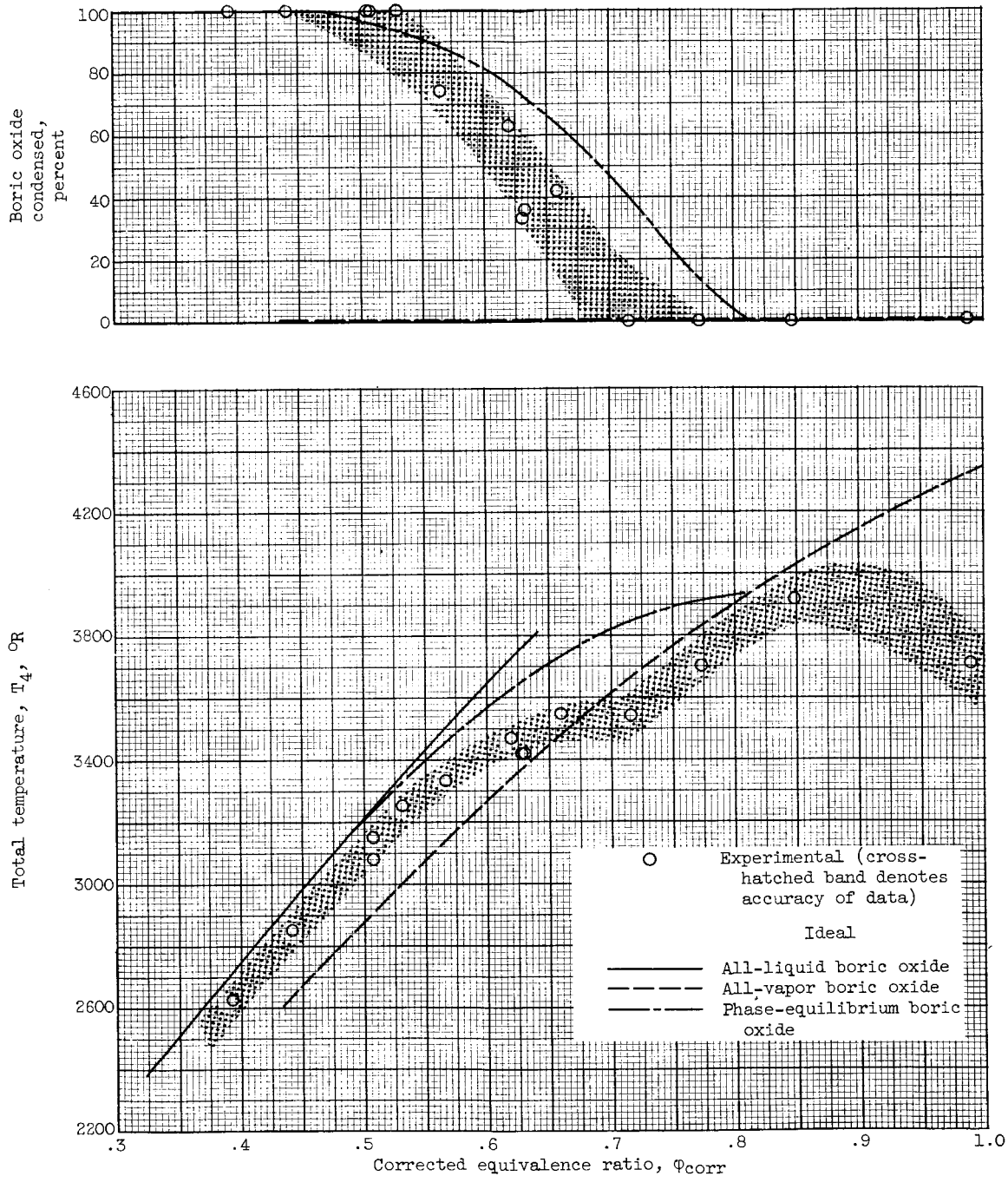

Figure 21. - Temperatures at exit of 8-inch-diameter combustor computed from ideal data and from experimental data. Fuel, HEF-2; combustor-inlet air temperature, 360° R; combustor pressure, 3 atmospheres.

DECLASSIFIED
CONFIDENTIAL

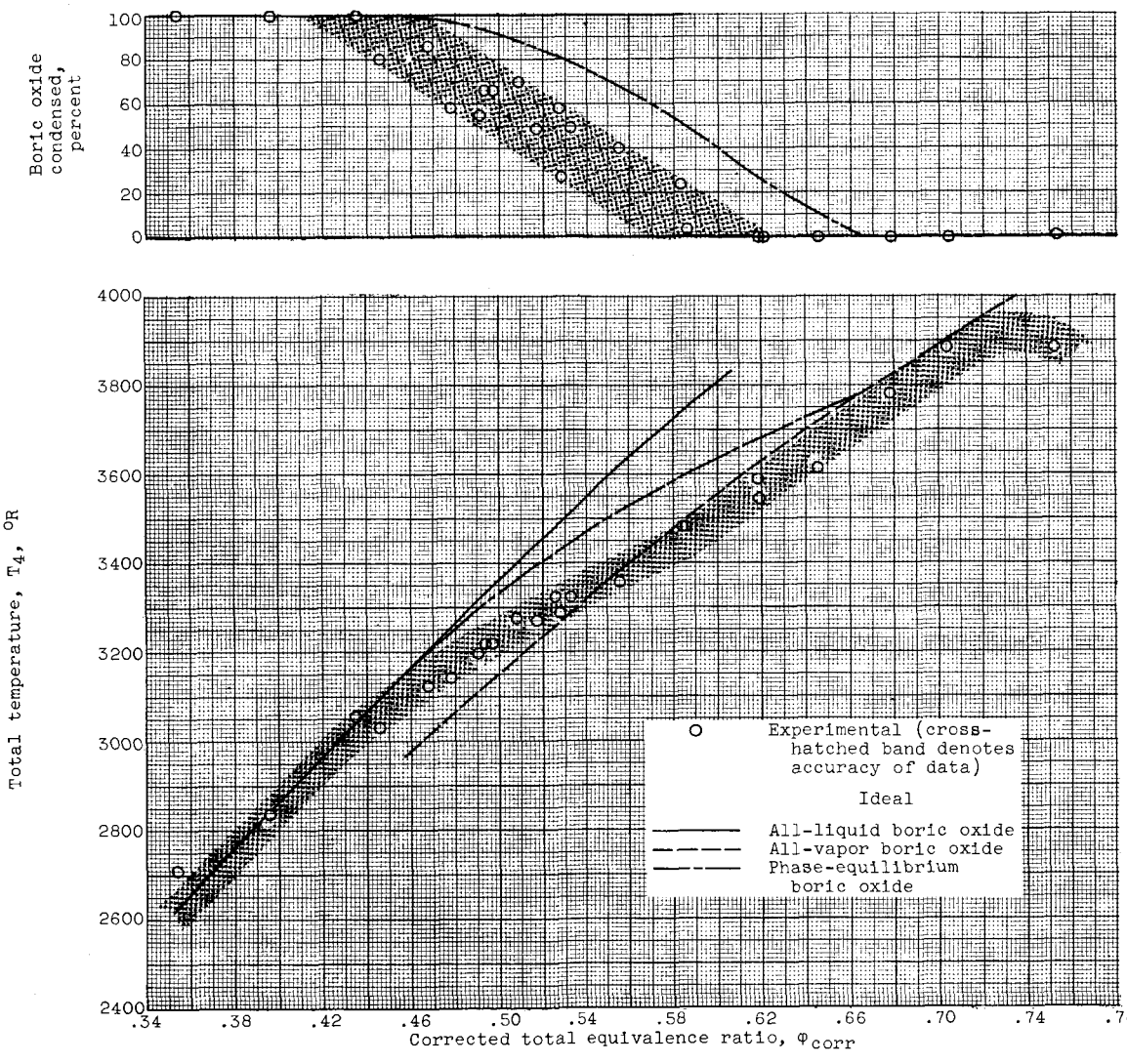

Figure 22. - Temperatures at exit of 28-inch-diameter afterburner computed from ideal data and experimental data. Primary-burner fuel, JP-4 at approximate equivalence ratio of 0.2; afterburner fuel, HEF-2; primary-burner-inlet air temperature, 844° R; combustor pressure, $2\frac{1}{2}$ atmospheres.

CONFIDENTIAL

CONFIDENTIAL

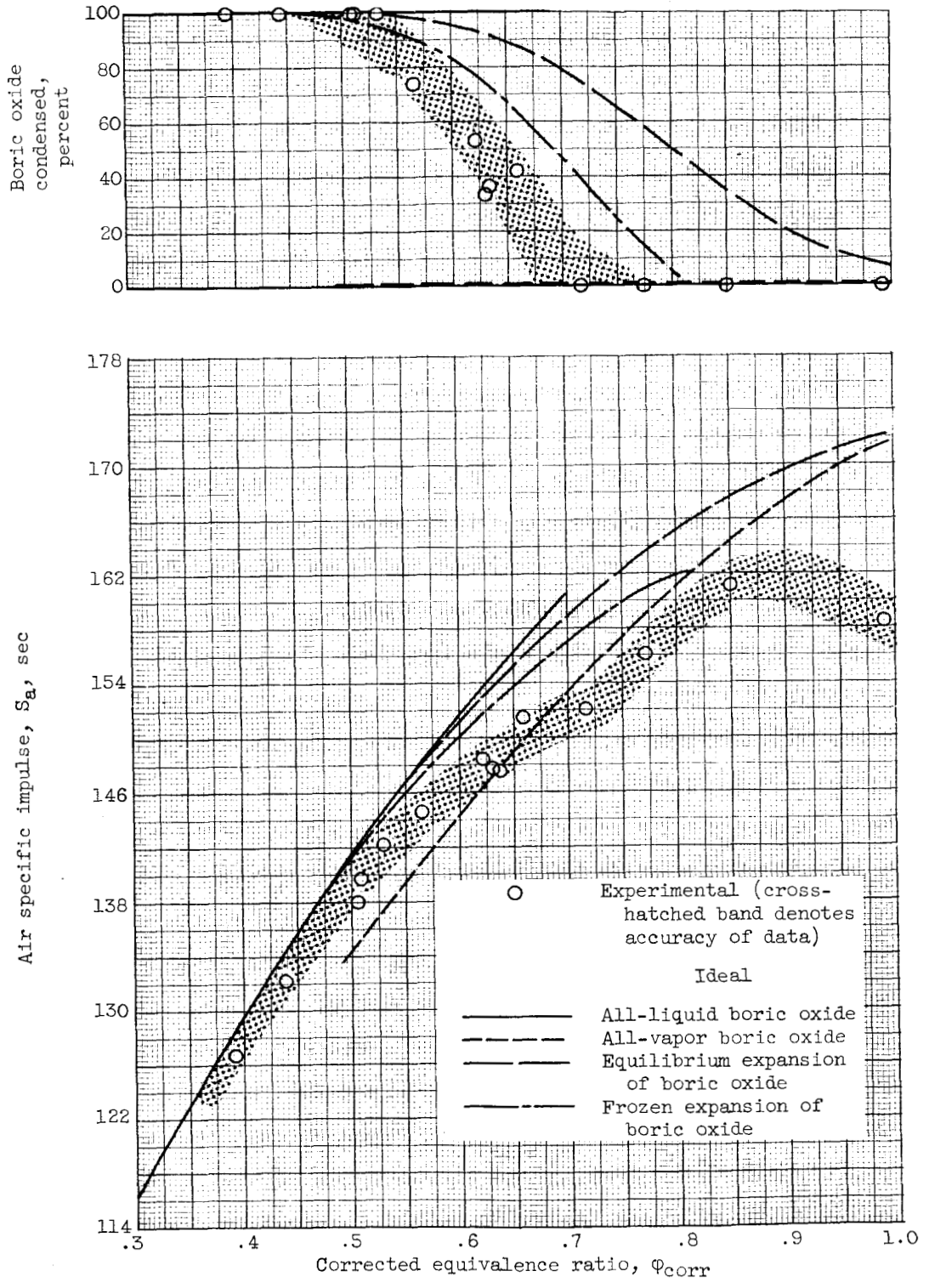

Figure 23. - Air specific impulse at nozzle throat of 8-inch-diameter combustor. Fuel, HEF-2; combustor-inlet air temperature, 360° R; combustor pressure, 3 atmospheres.

DECLASSIFIED

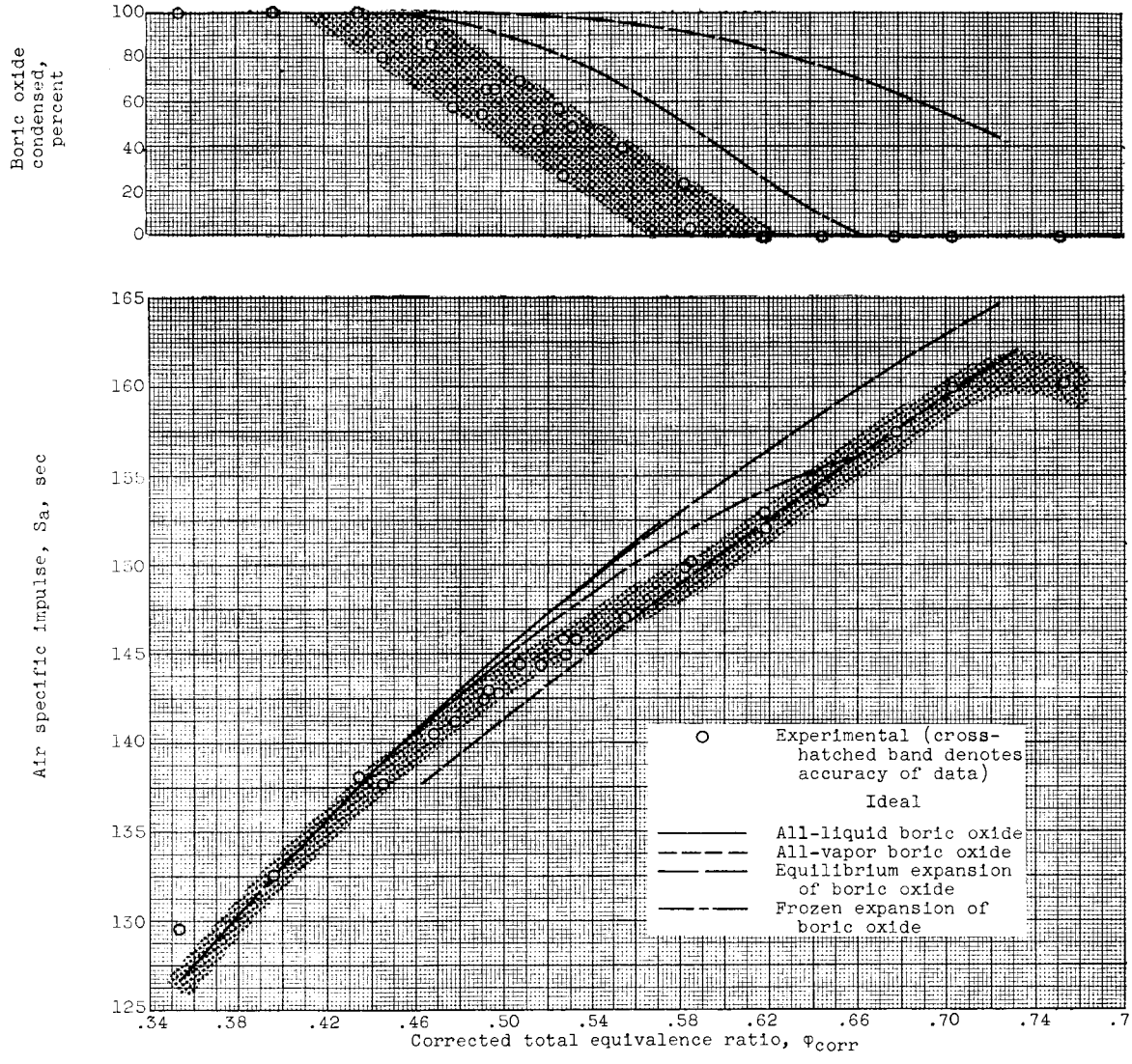

Figure 24. - Air specific impulse at nozzle throat of 28-inch-diameter afterburner. Primary-burner fuel, JP-4 at approximate equivalence ratio of 0.2; afterburner fuel, HEF-2; primary-burner-inlet air temperature, 844° R; combustor pressure, $2\frac{1}{2}$ atmospheres.

CONFIDENTIAL

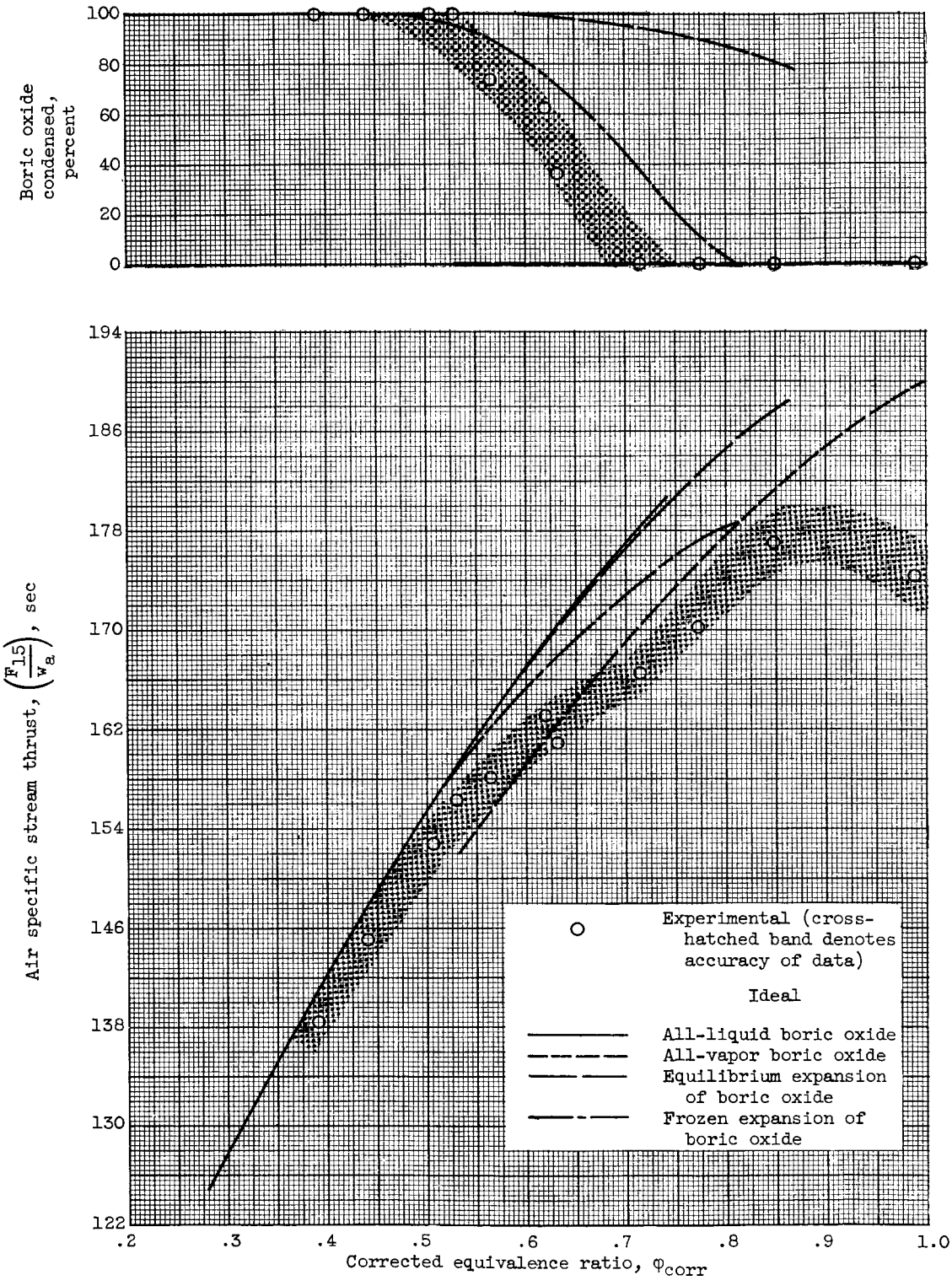

Figure 25. - Air specific stream thrust at nozzle exit of 8-inch-diameter combustor. Fuel, HEF-2; combustor-inlet air temperature, 360° R; combustor pressure, 3 atmospheres.

CONFIDENTIAL

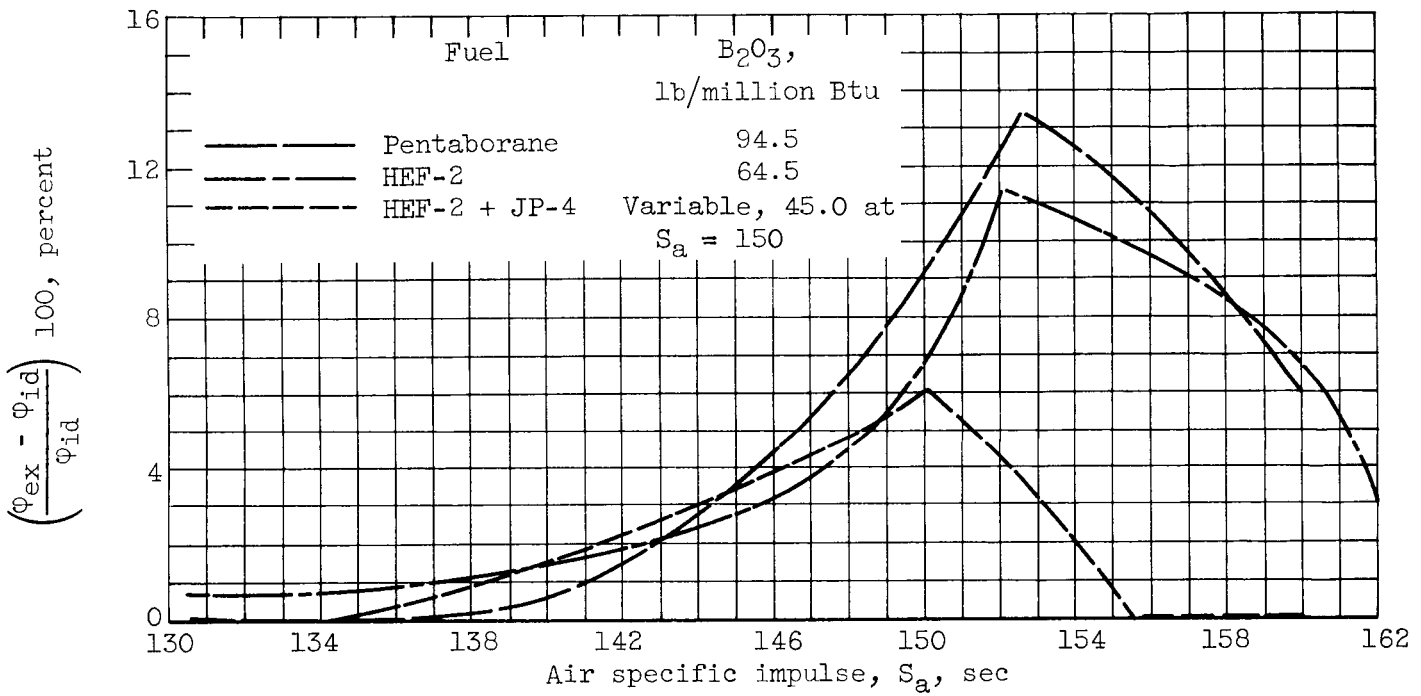

Figure 26. - Deviation of experimental fuel consumption from ideal when ideal model assumes frozen expansion of B_2O_3. Experimental equivalence ratios corrected to 100-percent combustion efficiency.

CONFIDENTIAL

CONFIDENTIAL

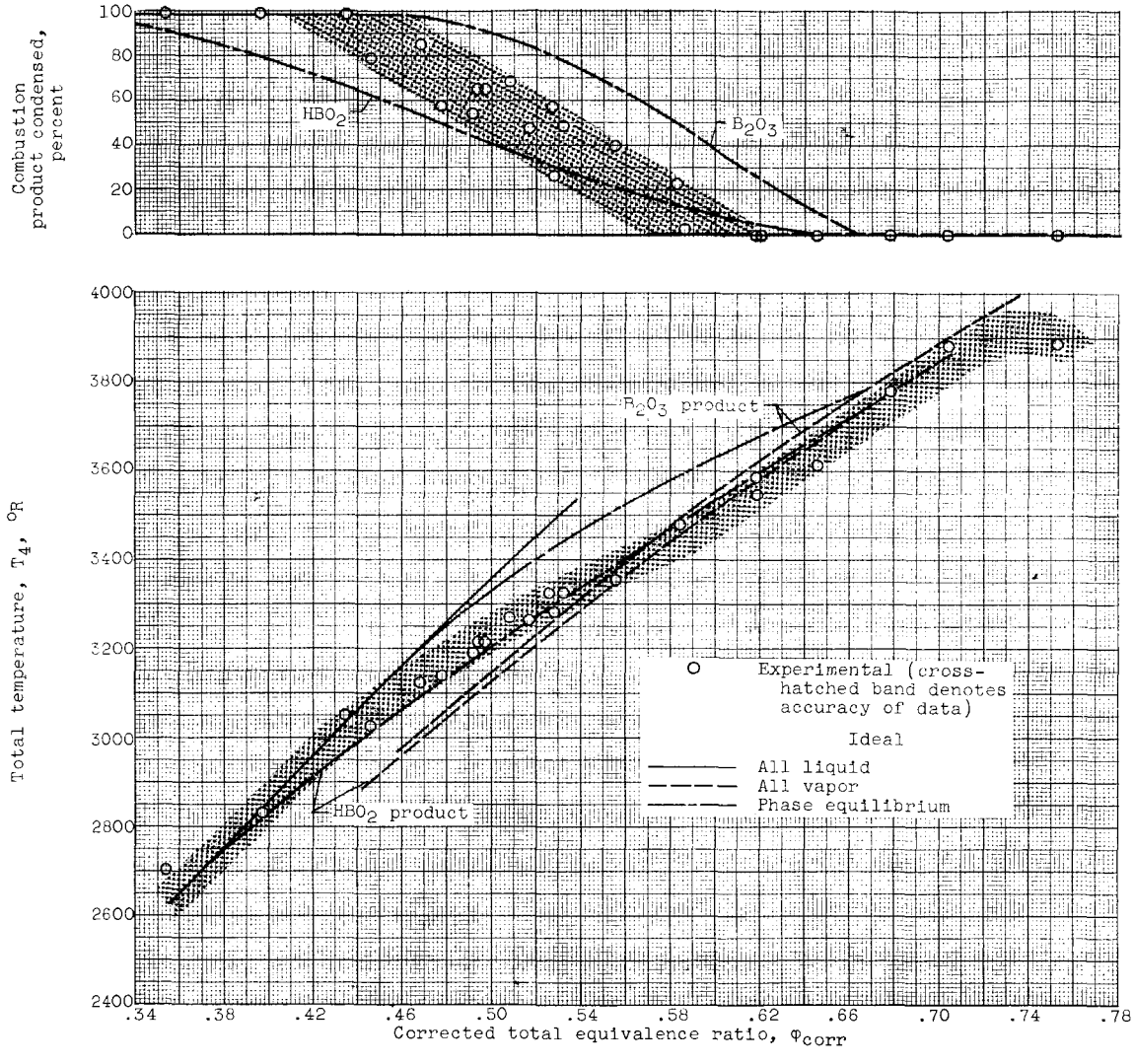

Figure 27. - Comparison of ideal temperatures computed for HBO_2 products with data of figure 22.

CONFIDENTIAL

DECLASSIFIED
CONFIDENTIAL

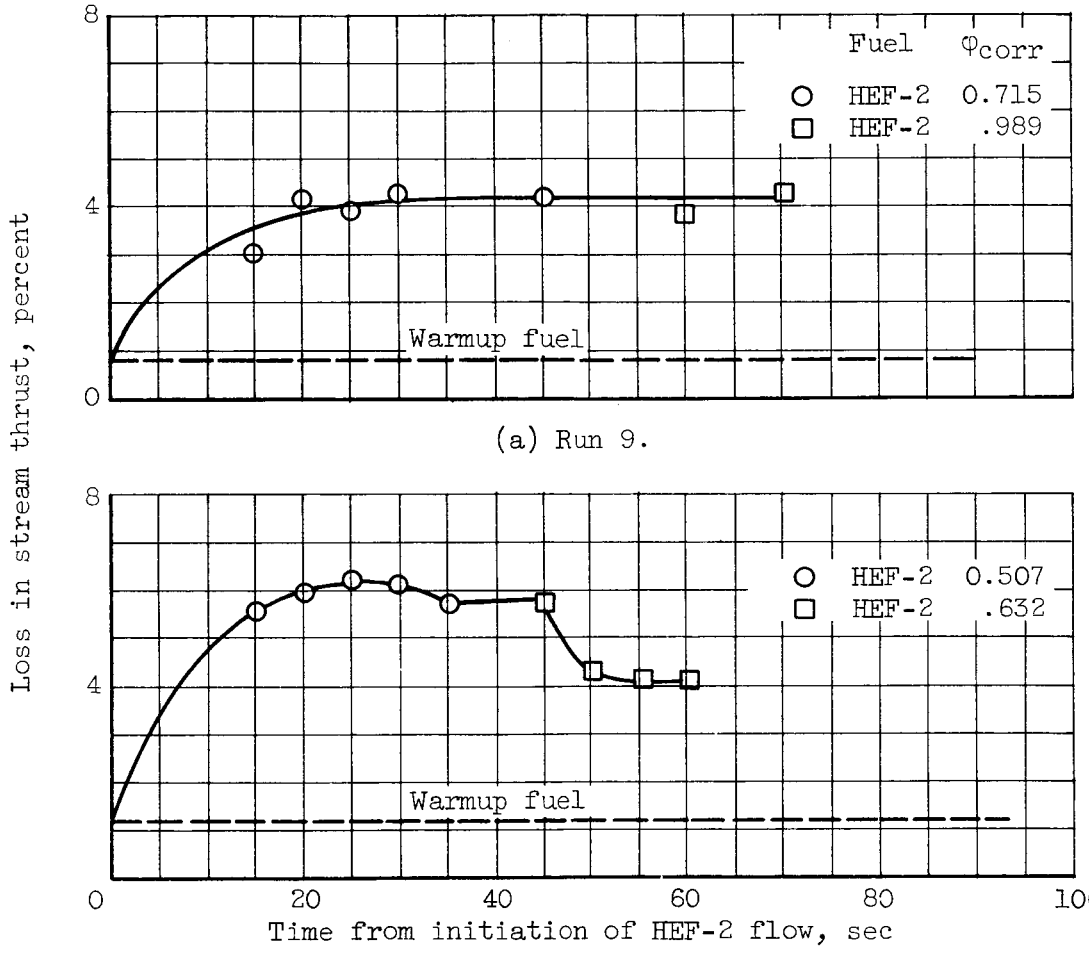

(a) Run 9.

(b) Run 11.

Figure 28. - Stream thrust loss resulting from frictional resistance of boric oxide films in exhaust nozzle of 8-inch-diameter combustor.

CONFIDENTIAL